JOURNAL OF GUIDANCE, CONTROL, AND DYNAMICS
Vol. 34, No. 1, January–February 2011

Dynamics and Control of a Biomimetic Vehicle Using Biased Wingbeat Forcing Functions

Michael W. Oppenheimer,* David B. Doman,† and David O. Sigthorsson‡
U.S. Air Force Research Laboratory, Wright-Patterson Air Force Base, Ohio 45433-7531

DOI: 10.2514/1.49735

A wingbeat forcing function and control method are presented that allow six-degree-of-freedom control of a flapping-wing micro air vehicle using only two actuators, each of which independently actuate a wing. Split-cycle constant-period frequency modulation with wing bias is used to produce nonzero cycle-averaged drag. The wing bias provides pitching-moment control and, when coupled with split-cycle constant-period frequency modulation, requires only independently actuated wings to enable six-degree-of-freedom flight. Wing bias shifts the cycle-averaged center-of-pressure locations of the wings, thus providing the ability to pitch the vehicle. Implementation of the wing bias is discussed, and modifications to the wingbeat forcing function are made to maintain wing position continuity. Instantaneous and cycle-averaged forces and moments are computed, cycle-averaged control derivatives are calculated, and a controller is developed. The controller is designed using a simplified aerodynamic model derived with blade-element theory and cycle averaging. The controller is tested using a simulation that includes blade-element-based estimates of the instantaneous aerodynamic forces and moments that are generated by the combined motion of the rigid-body fuselage and the flapping wings. Simulations using this higher-fidelity model indicate that the cycle-averaged blade-element-based controller is capable of achieving controlled flight.

Nomenclature

$\mathbf{B_{A1}}$	=	control effectiveness matrix
$\mathbf{B_{A1}}^{+}$	=	pseudoinverse of the control effectiveness matrix
$\mathbf{B_{A2}}$	=	sensitivity matrix due to prior wingbeat bias values
$C_D(\cdot)$, $C_D(\cdot)$	=	right and left wing drag coefficients
$C_L(\cdot)$, $C_L(\cdot)$	=	right and left wing lift coefficients
$D_{u_{\mathrm{LW}}}(t)$, $D_{d_{\mathrm{LW}}}(t)$	=	upstroke and downstroke left wing drag force
$D_{u_{\mathrm{RW}}}(t)$, $D_{d_{\mathrm{RW}}}(t)$	=	upstroke and downstroke right wing drag force
$\mathrm{d}D_{\mathrm{RW}}$, $\mathrm{d}D_{\mathrm{LW}}$	=	differential drag forces in relative wind velocity frames
$\mathrm{d}\mathbf{F}^{\mathrm{RRWV}}_{\mathrm{aero_{RW}}}(r)$, $\mathrm{d}\mathbf{F}^{\mathrm{LRWV}}_{\mathrm{aero_{LW}}}(r)$	=	differential force vectors in relative wind velocity frames
$\mathrm{d}\mathbf{F}^{\mathrm{RS}}_{\mathrm{aero_{RW}}}(r)$, $\mathrm{d}\mathbf{F}^{\mathrm{LS}}_{\mathrm{aero_{LW}}}(r)$	=	vectors of differential forces in spar frames
$\mathrm{d}L_{\mathrm{RW}}$, $\mathrm{d}L_{\mathrm{LW}}$	=	differential lift forces in relative wind velocity frames
$\mathrm{d}\mathbf{M}^{B}_{\mathrm{aero_{RW}}}(r)$, $\mathrm{d}\mathbf{M}^{B}_{\mathrm{aero_{LW}}}(r)$	=	vectors of differential moments in body frame
$\mathbf{F}^{B}_{u_{\mathrm{LW}}}(t)$, $\mathbf{F}^{B}_{d_{\mathrm{LW}}}(t)$	=	left wing upstroke and downstroke aerodynamic forces in body frame
$\mathbf{F}^{B}_{u_{\mathrm{RW}}}(t)$, $\mathbf{F}^{B}_{d_{\mathrm{RW}}}(t)$	=	right wing upstroke and downstroke aerodynamic forces in body frame
$H_n(\cdot)$	=	Struve function of order n
I_A	=	area moment of inertia of wing planform about wing root
$J_n(\cdot)$	=	Bessel function of order n
$L_{u_{\mathrm{LW}}}(t)$, $L_{d_{\mathrm{LW}}}(t)$	=	upstroke and downstroke left wing lift force
$L_{u_{\mathrm{RW}}}(t)$, $L_{d_{\mathrm{RW}}}(t)$	=	upstroke and downstroke right wing lift force
$\mathbf{M}^{B}_{u_{\mathrm{RW}}}(t)$	=	right wing upstroke aerodynamic moment in body frame
$\bar{M}^{B}_{x\mathrm{RW}}$, $\bar{M}^{B}_{x\mathrm{LW}}$	=	right and left cycle-averaged moments about the x-body axis
$\bar{M}^{B}_{y\mathrm{RW}}$, $\bar{M}^{B}_{y\mathrm{LW}}$	=	right and left cycle-averaged moments about the y-body axis
$\bar{M}^{B}_{z\mathrm{RW}}$, $\bar{M}^{B}_{z\mathrm{LW}}$	=	right and left cycle-averaged moments about the z-body axis
$\mathbf{R}^{\mathrm{RRWV}}_{\mathrm{RS}}$, $\mathbf{R}^{\mathrm{LRWV}}_{\mathrm{LS}}$	=	rotation matrices from spar frames to relative wind velocity frames
$\mathbf{R}^{\mathrm{RS}}_{\mathrm{RW}P}$, $\mathbf{R}^{\mathrm{LS}}_{\mathrm{LW}P}$	=	rotation matrices from wing planform frames to spar frames
$\mathbf{R}^{\mathrm{RS}}_{\mathrm{RW}R}$, $\mathbf{R}^{\mathrm{LS}}_{\mathrm{LW}R}$	=	rotation matrices from wing root frames to spar frames
r	=	point along wing spar measured from wing root
$\mathbf{r}^{B}_{p_{\mathrm{RW}}}$, $\mathbf{r}^{B}_{p_{\mathrm{LW}}}$	=	vectors from wing root to blade-element center of pressure
$\mathbf{v}^{B}_{b}$	=	body translational velocity in the body frame
$\mathbf{v}^{\mathrm{RS}}_{F_{\mathrm{RW}}}$, $\mathbf{v}^{\mathrm{LS}}_{F_{\mathrm{LW}}}$	=	velocities of wings due to flapping in right and left spar frames
$\mathbf{v}^{\mathrm{RS}}_{R_{\mathrm{RW}}}$, $\mathbf{v}^{\mathrm{LS}}_{R_{\mathrm{LW}}}$	=	velocities of wings due to rigid-body rotation in right and left spar frames
$\mathbf{v}^{\mathrm{RS}}_{\mathrm{RW}}$, $\mathbf{v}^{\mathrm{LS}}_{\mathrm{LW}}$	=	total velocities of wings written in right and left spar frames
$\mathbf{v}^{\mathrm{RS}}_{T_{\mathrm{RW}}}$, $\mathbf{v}^{\mathrm{LS}}_{T_{\mathrm{LW}}}$	=	velocities of wings due to rigid-body translation in right and left spar frames
$\mathbf{v}_{\infty_{\mathrm{RW}}}$, $\mathbf{v}_{\infty_{\mathrm{LW}}}$	=	velocity vectors consisting of the x and z components of $-\mathbf{v}^{\mathrm{RS}}_{\mathrm{RW}}$ and $-\mathbf{v}^{\mathrm{LS}}_{\mathrm{LW}}$
$\bar{X}^{B}_{\mathrm{RW}}$, $\bar{X}^{B}_{\mathrm{LW}}$	=	right and left cycle-averaged x-body axis forces
$[x^{\mathrm{WP}}_{\mathrm{cp}}, y^{\mathrm{WP}}_{\mathrm{cp}}, 0]^T$	=	location of wing center of pressure in local wing planform frame
$\bar{Y}^{B}_{\mathrm{RW}}$, $\bar{Y}^{B}_{\mathrm{LW}}$	=	right and left cycle-averaged y-body axis forces

Received 5 March 2010; revision received 4 October 2010; accepted for publication 4 October 2010.

*Senior Electronics Engineer, Control Design and Analysis Branch, 2210 Eighth Street, Building 146, Room 305; Michael.Oppenheimer@wpafb.af.mil. Associate Fellow AIAA.

†Senior Aerospace Engineer, Control Design and Analysis Branch, 2210 Eighth Street, Building 146, Room 305; David.Doman@wpafb.af.mil. Associate Fellow AIAA.

‡Electronics Engineer, Control Design and Analysis Branch, 2210 Eighth Street, Building 146, Room 305; David.Sigthorsson@gdit.com. Member AIAA.

$\bar{Z}^B_{\mathrm{RW}}, \bar{Z}^B_{\mathrm{LW}}$ = right and left cycle-averaged z-body axis forces
α = angle between stoke plane and wing chord; set by passive rotation joint
$\alpha_{\mathrm{RW}}, \alpha_{\mathrm{LW}}$ = smallest angle from x axis of right and left relative wind velocity coordinate frames to wing chord
$\alpha_{v_{\mathrm{RW}}}, \alpha_{v_{\mathrm{LW}}}$ = angles to transform from spar frames to relative wind velocity frames
$\alpha_{w_{\mathrm{RW}}}, \alpha_{w_{\mathrm{LW}}}$ = angle between the positive x axis of a spar frame and wing chord
$\Delta A_{\mathrm{LW}}, \Delta A_{\mathrm{RW}}$ = left and right wing amplitude adjustment terms
$\Delta\bar{F}^B_{x\mathrm{des}}, \Delta\bar{F}^B_{y\mathrm{des}}, \Delta\bar{F}^B_{z\mathrm{des}}$ = desired cycle-averaged forces
$\Delta\bar{M}^B_{x\mathrm{des}}, \Delta\bar{M}^B_{y\mathrm{des}}, \Delta\bar{M}^B_{z\mathrm{des}}$ = desired cycle-averaged moments
$\Delta\mathbf{r}^B_{\mathrm{LW}}$ = vector from center of gravity to left wing root in body frame, $[\,\Delta x^B_{\mathrm{LW}} \quad -\frac{w}{2} \quad \Delta z^B_{\mathrm{LW}}\,]$
$\Delta\mathbf{r}^B_{\mathrm{RW}}$ = vector from center of gravity to right wing root in body frame, $[\,\Delta x^B_{\mathrm{RW}} \quad \frac{w}{2} \quad \Delta z^B_{\mathrm{RW}}\,]$
$\delta_{\mathrm{LW}}, \delta_{\mathrm{RW}}$ = left and right wing upstroke split-cycle parameters
$\eta_{\mathrm{LW}}, \eta_{\mathrm{RW}}$ = left and right wing biases
$\eta_{\mathrm{LW}-1}, \eta_{\mathrm{RW}-1}$ = one-cycle-delayed left and right wing biases
$\xi_{\mathrm{LW}}, \xi_{\mathrm{RW}}$ = left and right wing phase shifts
ρ = atmospheric density
$\sigma_{\mathrm{LW}}, \sigma_{\mathrm{RW}}$ = left and right wing downstroke split-cycle parameters
$\phi_{u_{\mathrm{LW}}}(t), \phi_{d_{\mathrm{LW}}}(t)$ = wingbeat forcing functions for left wing during upstroke and downstroke
$\phi_{u_{\mathrm{RW}}}(t), \phi_{d_{\mathrm{RW}}}(t)$ = wingbeat forcing functions for right wing during upstroke and downstroke
w = vehicle width
$\omega_{\mathrm{LW}}, \omega_{\mathrm{RW}}$ = left and right wing fundamental frequencies
ω_o = trim frequency
$\boldsymbol{\omega}^B_b$ = body rotational velocity expressed in the body coordinate frame, $[\,P \quad Q \quad R\,]^T$

I. Introduction

FOR years, researchers have been interested and intrigued by the flight of flapping-wing insects. Some of the earliest research efforts on flapping-wing vehicle flight took place in the 1950s and 1960s [1–4]. Osborne [1] used blade-element analysis to represent the forces on a flapping wing. Jensen [2] studied the flight of locusts, while Vogel [3,4] analyzed the fruit fly and calculated a lift coefficient for this insect. More recently, flapping-wing micro air vehicles (MAVs) have received a great deal of interest from the research community due to their potential to achieve insectlike maneuverability [5–11]. The ability to mimic the flight behavior of insects could enable such a vehicle to perform missions that larger, fixed-wing vehicles are unable to perform, such as intelligence, surveillance, and reconnaissance in urban environments and indoor locations. These potential capabilities have prompted continued research into flapping-wing flight dynamics, control law development [12,13], and fabrication [7,8].

Biologists have been interested in insect flight for some time. Ellington [9,14–18] provided detailed analysis of hovering insect flight, including kinematics, lift and power requirements, and aerodynamic mechanisms. Other researchers have studied the flight of butterflies [19], Diptera [20] insects, bumblebees [10,11], and the hawkmoth *Manduca sexta* [21–23]. The motivation for these studies was to characterize and understand the mechanisms that enable insect flight.

The aerodynamics of flapping-wing flight are complex [9,14–18,24–27]. Wing–wing interactions, wake capture, leading-edge vortices, wing rotation, and acceleration are examples of some of the complex phenomena that occur. Dickinson and Götz [28] have studied the unsteady aerodynamics of model wings at low Reynolds numbers. Sane and Dickinson [6] have performed low-Reynolds-number experiments on rigid flapping wings in a mineral oil tank and proposed a quasi-steady aerodynamic model of the wing, while Sitaraman et al. [29] developed a numerical model of the unsteady aerodynamics of flapping flight.

Cycle-averaged control laws [12,13,30,31] for flapping-wing MAVs have been developed in the past. These control strategies used wing-flip timing and mean angle of attack as control variables or included an additional control effector to adjust the center of gravity of the vehicle. The control strategy introduced by Deng et al. [13] required four actuators, while split-cycle constant-period frequency modulation (SCCPFM) [13] was used to control a six-degree-of-freedom (DOF) unsteady simulation model of a flapping-wing MAV using three actuators; two actuators controlled wing position while the third controlled a bobweight. Wood [7] has stated that actuators can comprise 60% or more of the total weight of a flapping-wing MAV. Hence, a methodology is desired that would provide a high level of control for these types of vehicles, using as few actuators as possible. This work directly addresses this objective by developing a scheme that provides 6-DOF control using only two physical actuators. The vehicle selected for this study is similar to the RoboFly [7]. The key difference is that the wings are independently actuated [12] on the proposed vehicle, as shown in Fig. 1. Additional information about the vehicle, including a discussion of the passive-wing rotation joints as well as coordinate frame definitions, is given by Doman et al. [12]. Wood [7,8] and Wood et al. [32] have shown that tethered liftoff can be achieved with these types of vehicles. Here, a control strategy is presented that provides a wingbeat forcing function and control law that yields controlled 6-DOF flight of the vehicle using two physical actuators: one to drive the position of each wing. This is accomplished by using a biased version of the SCCPFM technique [12]. The bias has the effect of shifting the cycle-averaged center-of-pressure location of each wing, relative to the center of gravity, and provides the ability to manipulate the cycle-averaged pitching moment. With this technique, the need for a bobweight and its actuator used in previous studies [12] is eliminated, resulting in significant weight and complexity savings. A simplified aerodynamic model, which does not take into account unsteady effects, rigid-body translation, or rigid-body rotation, is used for control law design. The control law is tested for robustness by using a simulation model that includes blade-element-based estimates of the instantaneous aerodynamic forces and moments generated by the combined motion of the rigid-body fuselage and flapping wings relative to quiescent air surrounding the vehicle.

This paper is organized as follows. Section II explains the SCCPFM with bias technique. The blade-element aerodynamic model and the aerodynamic model with quasi-steady force coefficients and rigid-body translation and rotation are described in Sec. III, while cycle-averaged forces and moments are calculated in Sec. IV. The sensitivities of the cycle-averaged forces and moments to changes in the control parameters are computed in Sec. V, while the control derivatives about hover are calculated in Sec. VI. Section VII contains simulation results, and conclusions are provided in Sec. VIII.

II. Split-Cycle Constant-Period Frequency Modulation with Wing Bias

The wingbeat position command structure presented by Doman et al. [12] was shown to be capable of producing desired cycle-averaged horizontal and vertical forces as well as rolling and yawing moments. The inability of that control strategy to independently generate pitching moments led to the addition of a bobweight actuator, which was used to adjust the center of gravity of the vehicle and provided independent control of the pitching moment. In this work, a wing position bias is introduced that enables the cycle-averaged centers of pressure of the beating wings to be shifted, relative to the vehicle center of gravity, such that cycle-averaged pitching moments can be generated without a bobweight. The main contribution of this work is the ability to eliminate the need for the

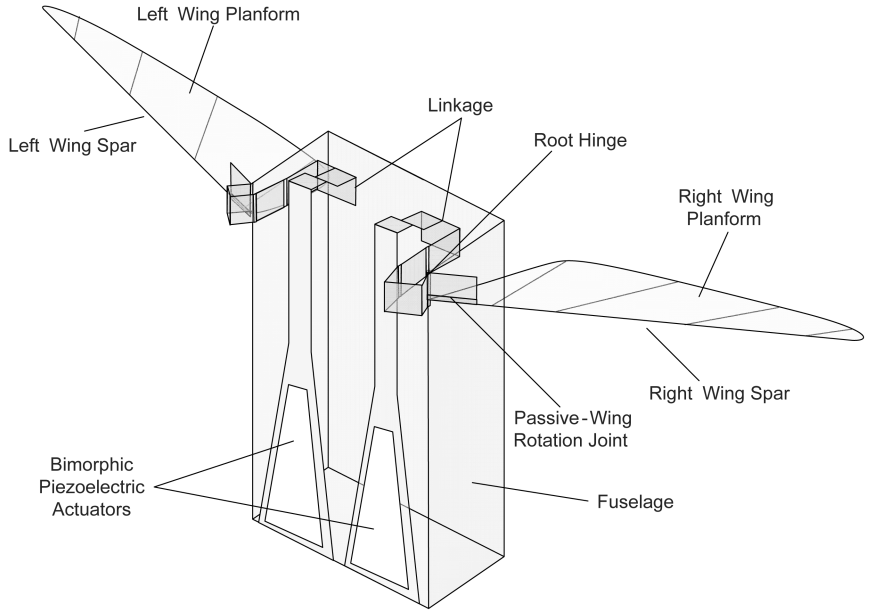

Fig. 1 General assembly of a minimally actuated flapping-wing MAV.

bobweight controller and actuator, which results in significant weight savings and a less complex vehicle design. It will be shown that the new control strategy is capable of generating six independent forces and moments using only two physical actuators. In this section, a wing bias is introduced into the wingbeat forcing functions.

The wingbeat forcing functions, which command the position of each wing during each beat cycle, are

$$\phi_{u_{\mathrm{LW}}}(t) = \cos[(\omega_{\mathrm{LW}} - \delta_{\mathrm{LW}})t] + \eta_{\mathrm{LW}}$$
$$\phi_{d_{\mathrm{LW}}}(t) = \cos[(\omega_{\mathrm{LW}} + \sigma_{\mathrm{LW}})t + \xi_{\mathrm{LW}}] + \eta_{\mathrm{LW}} \quad (1)$$

and

$$\phi_{u_{\mathrm{RW}}}(t) = \cos[(\omega_{\mathrm{RW}} - \delta_{\mathrm{RW}})t] + \eta_{\mathrm{RW}}$$
$$\phi_{d_{\mathrm{RW}}}(t) = \cos[(\omega_{\mathrm{RW}} + \sigma_{\mathrm{RW}})t + \xi_{\mathrm{RW}}] + \eta_{\mathrm{RW}} \quad (2)$$

where η_{RW} and η_{LW} are the wing biases, $\phi(t)$ is the wing position, the subscripts RW and LW denote the right and left wings, while u and d specify the upstroke and downstroke. For example, $\phi_{u_{\mathrm{LW}}}(t)$ is the wing position of the left wing during the upstroke. Without loss of generality, it is assumed that $t = 0$ at the beginning of each wingbeat cycle. In Eqs. (1) and (2), ω_{RW} and ω_{LW} are the fundamental or symmetric frequencies, δ_{RW} and δ_{LW} are the split-cycle parameters or asymmetric frequencies, $\sigma_{\mathrm{RW}} \triangleq \delta_{\mathrm{RW}}\omega_{\mathrm{RW}}/(\omega_{\mathrm{RW}} - 2\delta_{\mathrm{RW}})$, $\sigma_{\mathrm{LW}} \triangleq \delta_{\mathrm{LW}}\omega_{\mathrm{LW}}/(\omega_{\mathrm{LW}} - 2\delta_{\mathrm{LW}})$, $\xi_{\mathrm{RW}} \triangleq -2\pi\delta_{\mathrm{RW}}/(\omega_{\mathrm{RW}} - 2\delta_{\mathrm{RW}})$, and $\xi_{\mathrm{LW}} \triangleq -2\pi\delta_{\mathrm{LW}}/(\omega_{\mathrm{LW}} - 2\delta_{\mathrm{LW}})$ [12]. A complete derivation of the SCCPFM technique is provided by Doman et al. [12].

The addition of a wing bias decouples the z-body axis force and pitching moment to provide more control authority during the fore/aft fast translational portions of flight while, at the same time, it allows generation of direct side forces. Practical implementation requires that the bias terms be delayed by one full wingbeat cycle for reasons that will become evident shortly. Figure 2 shows the effects of changing the wing bias on the wingbeat forcing function. The wing bias is constrained to be constant over each full cycle, so that intercycle wing position discontinuities do not exist and the general cosine waveform shape is maintained. Maintaining a wingbeat position forcing function of a sinusoidal form allows closed-form solutions for the control derivatives. If the bias were allowed to vary within a wingbeat cycle, closed-form cycle-averaged control derivatives would be difficult, if not impossible, to compute. Thus, the wingstroke properties can only be adjusted at specific points within a cycle. If the wingstroke properties were adjustable only at the end of a cycle then, in general, since $\eta_0 \neq \eta_1 \neq \eta_2$, discontinuities would exist in the wing position, as shown in Fig. 2. This situation cannot be physically realized. To overcome this issue, the second half of the downstroke is modified by the addition of a cosine wave. For the first half of the downstroke, the wing position forcing function is exactly as shown in Eqs. (1) and (2). For the second half of the downstroke, the wing position forcing functions are modified to

$$\phi_{d_{\mathrm{LW}}}(t) = (1 + \Delta A_{\mathrm{LW}})\cos[(\omega_{\mathrm{LW}} + \sigma_{\mathrm{LW}})t + \xi_{\mathrm{LW}}] + \eta_{\mathrm{LW}} \quad (3)$$

and

$$\phi_{d_{\mathrm{RW}}}(t) = (1 + \Delta A_{\mathrm{RW}})\cos[(\omega_{\mathrm{RW}} + \sigma_{\mathrm{RW}})t + \xi_{\mathrm{RW}}] + \eta_{\mathrm{RW}} \quad (4)$$

The terms ΔA_{LW} and ΔA_{RW} adjust the amplitude of the wingbeat forcing function during the last half of the downstroke to maintain a continuous wingbeat position forcing function.

To calculate the amplitude adjustment terms, consider the end of a complete wingbeat cycle and, for brevity, consider only the left wing (right wing calculations are similar). Using Eq. (3), it can be seen that at the end of the first complete cycle, when $t = \frac{2\pi}{\omega}$, the modified downstroke wing position is

$$\phi_{d_{\mathrm{LW}}}(t)|_{t=2\pi/\omega} = 1 + \eta_{\mathrm{LW}_0} + \Delta A_{\mathrm{LW}_1} \quad (5)$$

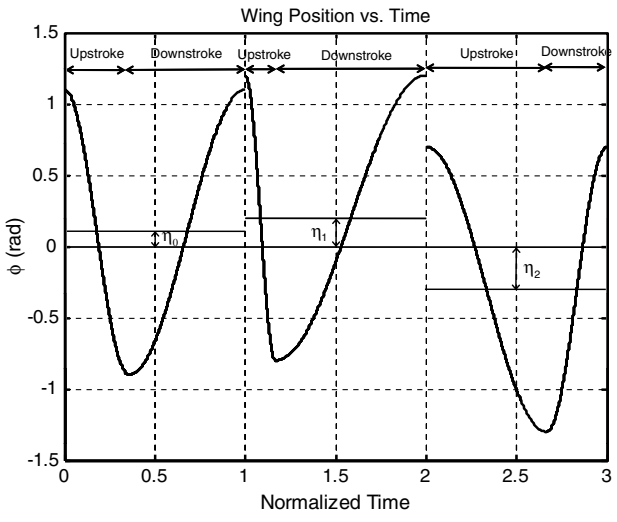

Fig. 2 Wing position with variable η.

while at the beginning of the second cycle upstroke, the wing position [Eq. (1)] is given by

$$\phi_{u_{\mathrm{LW}}}(t)|_{t=2\pi/\omega} = 1 + \eta_{\mathrm{LW}_1} \tag{6}$$

Setting Eq. (5) equal to Eq. (6) (to satisfy wing position continuity) and solving for ΔA_{LW_1} yields

$$\Delta A_{\mathrm{LW}_1} = \eta_{\mathrm{LW}_1} - \eta_{\mathrm{LW}_0} \tag{7}$$

In general, this expression becomes

$$\Delta A_i = \eta_i - \eta_{i-1} \tag{8}$$

Thus, in order to determine ΔA_i, the system needs information about the bias of the upcoming wingbeat cycle, which results in a practical requirement that wing bias changes be subject to a delay.

Figure 3 shows the points in the wingbeat cycle where ω_i, δ_i, η_i, and ΔA_i are calculated and applied. Note that these variables are calculated at the beginning of the upstroke and that ΔA_i is applied for the last half of the downstroke to ensure wing position continuity. The bias term is delayed by one full wingbeat cycle and is applied for the next complete wingbeat cycle. This ensures that all necessary data are available for the computation of ΔA_i. Thus, at the beginning of an upstroke, ω_i and δ_i are calculated and immediately applied for a complete cycle. Also, ΔA_i and η_i are calculated, with ΔA_i being applied for the last half of the current wingbeat downstroke and η_i being applied for the next full cycle.

In summary, the forcing functions driving the positions of the wings are as follows:

upstroke,

$$\begin{aligned}\phi_{u_{\mathrm{LW}}}(t) &= \cos[(\omega_{\mathrm{LW}} - \delta_{\mathrm{LW}})t] + \eta_{\mathrm{LW}};\\ \phi_{u_{\mathrm{RW}}}(t) &= \cos[(\omega_{\mathrm{RW}} - \delta_{\mathrm{RW}})t] + \eta_{\mathrm{RW}}\end{aligned} \tag{9}$$

first half of downstroke,

$$\begin{aligned}\phi_{d_{\mathrm{LW}}}(t) &= \cos[(\omega_{\mathrm{LW}} + \sigma_{\mathrm{LW}})t + \xi_{\mathrm{LW}}] + \eta_{\mathrm{LW}};\\ \phi_{d_{\mathrm{RW}}}(t) &= \cos[(\omega_{\mathrm{RW}} + \sigma_{\mathrm{RW}})t + \xi_{\mathrm{RW}}] + \eta_{\mathrm{RW}}\end{aligned}$$

second half of downstroke,

$$\begin{aligned}\phi_{d_{\mathrm{LW}}}(t) &= (1 + \Delta A_{\mathrm{LW}})\cos[(\omega_{\mathrm{LW}} + \sigma_{\mathrm{LW}})t + \xi_{\mathrm{LW}}] + \eta_{\mathrm{LW}};\\ \phi_{d_{\mathrm{RW}}}(t) &= (1 + \Delta A_{\mathrm{RW}})\cos[(\omega_{\mathrm{RW}} + \sigma_{\mathrm{RW}})t + \xi_{\mathrm{RW}}] + \eta_{\mathrm{RW}}\end{aligned}$$

where, without loss of generality, the time at the beginning of each wingbeat cycle is taken to be zero. In Eq. (9), the wingbeat segments are defined by the following times:

1) For the upstroke, $0 \le t < \pi/(\omega - \delta)$.

2) For the first half of the downstroke, $\pi/(\omega - \delta) \le t < [\pi(3\omega - 2\delta)]/[2\omega(\omega - \delta)]$.

3) For the second half of the downstroke, $[\pi(3\omega - 2\delta)]/[2\omega(\omega - \delta)] \le t < 2\pi/\omega$.

In Eq. (9), the time index subscripts on the variables are omitted for brevity. It should be understood that, for wingbeat cycle i, the biases used are $\eta_{\mathrm{LW}_{i-1}}$ and $\eta_{\mathrm{RW}_{i-1}}$, while the fundamental frequencies ω_{RW} and ω_{LW}, the split-cycle parameters δ_{RW} and δ_{LW}, and the amplitude modification parameters ΔA_{RW} and ΔA_{LW} are the current time values.

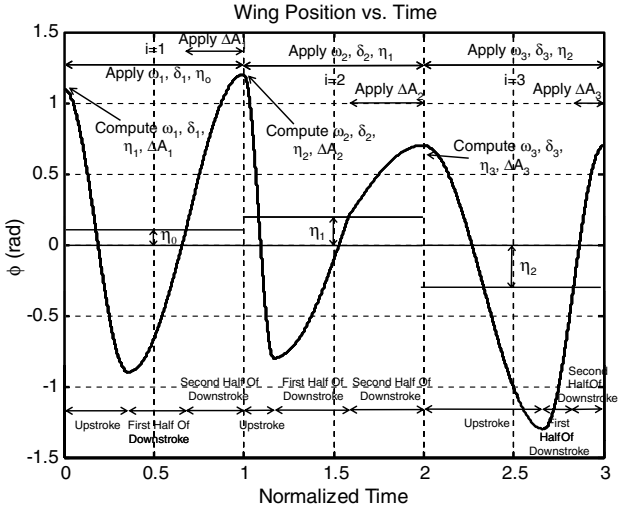

Fig. 3 Points in wingbeat cycle where control parameters are calculated and applied.

III. Aerodynamic Models of a Flapping-Wing Vehicle with Independently Actuated Wings

In this section, two aerodynamic models of the flapping-wing vehicle are discussed. One of the objectives of this work is to develop a model that yields insight into the controllability of this class of vehicles. In light of this objective, the first aerodynamic model is void of any unsteady aerodynamic effects, does not consider rigid-body motion of the fuselage relative to the surrounding air, and is based on blade-element theory. The use of computational fluid dynamics or finite element models would provide a higher-fidelity model; however, these techniques would not allow designers to make vehicle modifications and rapidly assess their effects. Thus, they have a tendency to mask the most pertinent factors in force and moment generation. An additional benefit of the simplified aerodynamic model is the ability to analytically compute cycle-averaged control derivatives for use in the control law (which would most likely not be possible using a higher-fidelity aerodynamic model) without expending considerable computational resources. This reduced order or cycle-averaged blade-element aerodynamic model is solely used for control law development and tuning. The control law, based on a cycle-averaged blade-element aerodynamic model, is tested on a higher-fidelity model that includes an instantaneous blade-element estimate of the aerodynamic forces and moments due to the flapping wings and rigid-body translation and rotation of the fuselage relative to still air. The 6-DOF equations of motion, which determine the state of the vehicle during simulation, are driven by the instantaneous forces and moments from the higher-fidelity model. Both models will be discussed in the next sections. Before introducing the models, expressions for the lift, drag, and moments due to wing flapping are needed.

Using the relationships between the body, wing roots, spars, upstroke planform and downstroke planform axes systems established by Doman et al. [12], the instantaneous values of lift and drag on each wing may be transformed into a body axis coordinate frame. The aerodynamic forces, expressed in the body frame, associated with each wing and stroke are summarized in Table 1 (the superscript B denotes the body frame). $L(t)$ is the lift force and $D(t)$ is the drag force.

The instantaneous aerodynamic moment for the right wing during the upstroke is

$$\mathbf{M}^{B}_{u_{\mathrm{RW}}}(t) = \begin{bmatrix} D_{u_{\mathrm{RW}}}(t)\left[y^{\mathrm{WP}}_{\mathrm{cp}} + \frac{w}{2}\cos\phi_{u_{\mathrm{RW}}}(t) + \Delta z^{B}_{\mathrm{RW}}\sin\phi_{u_{\mathrm{RW}}}(t)\right] \\ L_{u_{\mathrm{RW}}}(t)[y^{\mathrm{WP}}_{\mathrm{cp}}\sin\phi_{u_{\mathrm{RW}}}(t) + \Delta z^{B}_{\mathrm{RW}}] - D_{u_{\mathrm{RW}}}(t)\Delta x^{B}_{\mathrm{RW}}\cos\phi_{u_{\mathrm{RW}}}(t) - [L_{u_{\mathrm{RW}}}(t)\cos\alpha + D_{u_{\mathrm{RW}}}(t)\sin\alpha]x^{\mathrm{WP}}_{\mathrm{cp}}\cos\phi_{u_{\mathrm{RW}}}(t) \\ -D_{u_{\mathrm{RW}}}(t)\Delta x^{B}_{\mathrm{RW}}\sin\phi_{u_{\mathrm{RW}}}(t) - L_{u_{\mathrm{RW}}}(t)\left[\frac{w}{2} + y^{\mathrm{WP}}_{\mathrm{cp}}\cos\phi_{u_{\mathrm{RW}}}(t)\right] - [L_{u_{\mathrm{RW}}}(t)\cos\alpha + D_{u_{\mathrm{RW}}}(t)\sin\alpha]x^{\mathrm{WP}}_{\mathrm{cp}}\sin\phi_{u_{\mathrm{RW}}}(t) \end{bmatrix} \tag{10}$$

Table 1 Instantaneous aerodynamic forces expressed in the body frame

Force	Body frame
RW upstroke	$\mathbf{F}^B_{u_{\mathrm{RW}}}(t) = \begin{bmatrix} L_{u_{\mathrm{RW}}}(t) \\ -D_{u_{\mathrm{RW}}}(t)\sin\phi_{u_{\mathrm{RW}}}(t) \\ D_{u_{\mathrm{RW}}}(t)\cos\phi_{u_{\mathrm{RW}}}(t) \end{bmatrix}$
RW downstroke	$\mathbf{F}^B_{d_{\mathrm{RW}}}(t) = \begin{bmatrix} L_{d_{\mathrm{RW}}}(t) \\ D_{d_{\mathrm{RW}}}(t)\sin\phi_{d_{\mathrm{RW}}}(t) \\ -D_{d_{\mathrm{RW}}}(t)\cos\phi_{d_{\mathrm{RW}}}(t) \end{bmatrix}$
LW upstroke	$\mathbf{F}^B_{u_{\mathrm{LW}}}(t) = \begin{bmatrix} L_{u_{\mathrm{LW}}}(t) \\ D_{u_{\mathrm{LW}}}(t)\sin\phi_{u_{\mathrm{LW}}}(t) \\ D_{u_{\mathrm{LW}}}(t)\cos\phi_{u_{\mathrm{LW}}}(t) \end{bmatrix}$
LW downstroke	$\mathbf{F}^B_{d_{LW}}(t) = \begin{bmatrix} L_{d_{LW}}(t) \\ -D_{d_{LW}}(t)\sin\phi_{d_{LW}}(t) \\ -D_{d_{LW}}(t)\cos\phi_{d_{LW}}(t) \end{bmatrix}$

where $\Delta\mathbf{r}^B_{\mathrm{RW}} = [\,\Delta x^B_{\mathrm{RW}} \quad \frac{w}{2} \quad \Delta z^B_{\mathrm{RW}}\,]$ is the position vector from the center of gravity to the origin of the right wing coordinate system, $x^{\mathrm{WP}}_{\mathrm{cp}}$ and $y^{\mathrm{WP}}_{\mathrm{cp}}$ define the location of the center of pressure in the local wing planform frame, and w is the width of the vehicle. Expressions for the aerodynamic moments for the right wing during a downstroke and the left wing during both strokes can be found in Doman et al. [12].

A. Blade-Element Aerodynamic Forces and Moments

Using a blade-element aerodynamic model, the instantaneous lift and drag of the left and right wings during the upstroke and downstroke are [12] as follows:

upstroke,

$$\begin{aligned} L_{u_{\mathrm{LW}}}(t) &= k_L(\omega_{\mathrm{LW}} - \delta_{\mathrm{LW}})^2\sin^2[(\omega_{\mathrm{LW}} - \delta_{\mathrm{LW}})t] \\ D_{u_{\mathrm{LW}}}(t) &= k_D(\omega_{\mathrm{LW}} - \delta_{\mathrm{LW}})^2\sin^2[(\omega_{\mathrm{LW}} - \delta_{\mathrm{LW}})t] \\ L_{u_{\mathrm{RW}}}(t) &= k_L(\omega_{\mathrm{RW}} - \delta_{\mathrm{RW}})^2\sin^2[(\omega_{\mathrm{RW}} - \delta_{\mathrm{RW}})t] \\ D_{u_{\mathrm{RW}}}(t) &= k_D(\omega_{\mathrm{RW}} - \delta_{\mathrm{RW}})^2\sin^2[(\omega_{\mathrm{RW}} - \delta_{\mathrm{RW}})t] \end{aligned} \tag{11}$$

first half of downstroke,

$$\begin{aligned} L_{d_{\mathrm{LW}}}(t) &= k_L(\omega_{\mathrm{LW}} + \sigma_{\mathrm{LW}})^2\sin^2[(\omega_{\mathrm{LW}} + \sigma_{\mathrm{LW}})t + \xi_{\mathrm{LW}}] \\ D_{d_{\mathrm{LW}}}(t) &= k_D(\omega_{\mathrm{LW}} + \sigma_{\mathrm{LW}})^2\sin^2[(\omega_{\mathrm{LW}} + \sigma_{\mathrm{LW}})t + \xi_{\mathrm{LW}}] \\ L_{d_{\mathrm{RW}}}(t) &= k_L(\omega_{\mathrm{RW}} + \sigma_{\mathrm{RW}})^2\sin^2[(\omega_{\mathrm{RW}} + \sigma_{\mathrm{RW}})t + \xi_{\mathrm{RW}}] \\ D_{d_{\mathrm{RW}}}(t) &= k_D(\omega_{\mathrm{RW}} + \sigma_{\mathrm{RW}})^2\sin^2[(\omega_{\mathrm{RW}} + \sigma_{\mathrm{RW}})t + \xi_{\mathrm{RW}}] \end{aligned}$$

second half of downstroke,

$$\begin{aligned} L_{d_{\mathrm{LW}}}(t) &= k_L(1 + \Delta A_{\mathrm{LW}})^2(\omega_{\mathrm{LW}} + \sigma_{\mathrm{LW}})^2 \\ &\quad \times \sin^2[(\omega_{\mathrm{LW}} + \sigma_{\mathrm{LW}})t + \xi_{\mathrm{LW}}] \\ D_{d_{\mathrm{LW}}}(t) &= k_D(1 + \Delta A_{\mathrm{LW}})^2(\omega_{\mathrm{LW}} + \sigma_{\mathrm{LW}})^2 \\ &\quad \times \sin^2[(\omega_{\mathrm{LW}} + \sigma_{\mathrm{LW}})t + \xi_{\mathrm{LW}}] \\ L_{d_{\mathrm{RW}}}(t) &= k_L(1 + \Delta A_{\mathrm{RW}})^2(\omega_{\mathrm{RW}} + \sigma_{\mathrm{RW}})^2 \\ &\quad \times \sin^2[(\omega_{\mathrm{RW}} + \sigma_{\mathrm{RW}})t + \xi_{\mathrm{RW}}] \\ D_{d_{\mathrm{RW}}}(t) &= k_D(1 + \Delta A_{\mathrm{RW}})^2(\omega_{\mathrm{RW}} + \sigma_{\mathrm{RW}})^2 \\ &\quad \times \sin^2[(\omega_{\mathrm{RW}} + \sigma_{\mathrm{RW}})t + \xi_{\mathrm{RW}}] \end{aligned}$$

where $k_L \triangleq \frac{\rho}{2}C_L(\alpha)I_A$, $k_D \triangleq \frac{\rho}{2}C_D(\alpha)I_A$, α is the angle between the stroke plane and the wing chord (set by the passive-wing rotation joint), $C_L(\alpha)$ and $C_D(\alpha)$ are the lift and drag coefficients, and I_A is the area moment of inertia of the planform about the wing root. The lift and drag are used in the expressions in Table 1 and Eq. (10) to compute the body frame forces and moments due to wing flapping.

B. Flapping-Wing Aerodynamic Model with Linear and Angular Velocity Effects

In addition to being a function of wing kinematics, the aerodynamic forces and moments produced by the wings are also functions of the angular and translational motion of the rigid body. The goal of this section is to compute forces and moments produced by the wings due to rigid-body motion and wing flapping. Both Hedrick et al. [33] and Faruque and Humbert [34] have discussed the importance of including angular and translational motion in the calculation of wing velocity. To increase the fidelity of the aerodynamic forces produced by the flapping-wing vehicle model, translational and rotational motion of the rigid body along with wing flapping are included in the calculation of the wing velocity. The wing is split into blade elements along the span. The velocity of each blade element, with respect to still air, is calculated. Note that blade elements along the span experience different angles of attack when flapping motion and rigid-body translational and rotational motion are considered. Thus, the angle of attack of each blade element is calculated separately. Using the blade-element velocities and angles of attack, the force (and moment) due to motion of each blade element is computed. Numerical integration along the spar provides the total force and moment produced by each wing. These instantaneous forces and moments are then used to drive the 6-DOF equations of motion. The empirically derived lift and drag coefficients from Sane and Dickinson [5] are used in the subsequent analysis.

The inclusion of rigid-body translation and rotation follows the work of Faruque and Humbert [34]. The objective is to determine the velocity of each wing. This velocity consists of three components and can be written as

$$\begin{aligned} \mathbf{v}^{\mathrm{RS}}_{\mathrm{RW}} &= \mathbf{v}^{\mathrm{RS}}_{F_{\mathrm{RW}}} + \mathbf{v}^{\mathrm{RS}}_{T_{\mathrm{RW}}} + \mathbf{v}^{\mathrm{RS}}_{R_{\mathrm{RW}}} = \begin{bmatrix} v^{\mathrm{RS}}_{\mathrm{RW}_x} & v^{\mathrm{RS}}_{\mathrm{RW}_y} & v^{\mathrm{RS}}_{\mathrm{RW}_z} \end{bmatrix} \\ \mathbf{v}^{\mathrm{LS}}_{\mathrm{LW}} &= \mathbf{v}^{\mathrm{LS}}_{F_{\mathrm{LW}}} + \mathbf{v}^{\mathrm{LS}}_{T_{\mathrm{LW}}} + \mathbf{v}^{\mathrm{LS}}_{R_{\mathrm{LW}}} = \begin{bmatrix} v^{\mathrm{LS}}_{\mathrm{LW}_x} & v^{\mathrm{LS}}_{\mathrm{LW}_y} & v^{\mathrm{LS}}_{\mathrm{LW}_z} \end{bmatrix} \end{aligned} \tag{12}$$

where $\mathbf{v}^{\mathrm{RS}}_{\mathrm{RW}}$ and $\mathbf{v}^{\mathrm{LS}}_{\mathrm{LW}}$ are the velocity of the right and left wings written in the right and left wing spar frames, and $\mathbf{v}^{\mathrm{RS}}_{F_{\mathrm{RW}}}$, $\mathbf{v}^{\mathrm{RS}}_{T_{\mathrm{RW}}}$, $\mathbf{v}^{\mathrm{RS}}_{R_{\mathrm{RW}}}$, $\mathbf{v}^{\mathrm{LS}}_{F_{\mathrm{LW}}}$, $\mathbf{v}^{\mathrm{LS}}_{T_{\mathrm{LW}}}$, and $\mathbf{v}^{\mathrm{LS}}_{R_{\mathrm{LW}}}$ are the wing velocities due to flapping (F), rigid-body translation (T), and rigid-body rotation (R) of the right and left wings, written in the right and left spar frames. The coordinate frames necessary for this analysis are defined by Doman et al. [12]. Superscripts on a vector indicate the frame in which the vector is expressed.

By reviewing the definition of the wing spar coordinate frames for the left and right wings [12], the wing velocity due to flapping becomes

$$\mathbf{v}^{\mathrm{RS}}_{F_{\mathrm{RW}}} = \begin{bmatrix} r\dot{\phi}_{\mathrm{RW}} \\ 0 \\ 0 \end{bmatrix}; \qquad \mathbf{v}^{\mathrm{LS}}_{F_{\mathrm{LW}}} = \begin{bmatrix} -r\dot{\phi}_{\mathrm{LW}} \\ 0 \\ 0 \end{bmatrix} \tag{13}$$

where r is a point along the wing spar.

The wing velocity component due to rigid-body translation of the fuselage is computed by simply converting the body velocity $\mathbf{v}^B_b$ to the spar frames. Therefore,

$$\mathbf{v}^{\mathrm{RS}}_{T_{\mathrm{RW}}} = \mathbf{R}^{\mathrm{RS}}_{\mathrm{RW}R}\mathbf{v}^B_b; \qquad \mathbf{v}^{\mathrm{LS}}_{T_{\mathrm{LW}}} = \mathbf{R}^{\mathrm{LS}}_{\mathrm{LW}R}\mathbf{v}^B_b \tag{14}$$

where $\mathbf{R}^{\mathrm{RS}}_{\mathrm{RW}R}$ and $\mathbf{R}^{\mathrm{LS}}_{\mathrm{LW}R}$ are rotation matrices from the right and left wing root coordinate frames to the right and left wing spar coordinate frames [12], respectively.

The wing velocity due to rigid-body fuselage rotation is

$$\mathbf{v}^{\mathrm{RS}}_{R_{\mathrm{RW}}}(r) = \mathbf{R}^{\mathrm{RS}}_{\mathrm{RW}R}(\boldsymbol{\omega}^B_b \times \boldsymbol{r}^B_{p\mathrm{RW}}); \qquad \mathbf{v}^{\mathrm{LS}}_{R_{\mathrm{LW}}}(r) = \mathbf{R}^{\mathrm{LS}}_{\mathrm{LW}R}(\boldsymbol{\omega}^B_b \times \boldsymbol{r}^B_{p\mathrm{LW}}) \tag{15}$$

where $\boldsymbol{\omega}^B_b = [\,P \quad Q \quad R\,]^T$ is the body rotational velocity expressed in the body coordinate frame and $\boldsymbol{r}^B_{p\mathrm{RW}}$ and $\boldsymbol{r}^B_{p\mathrm{LW}}$ are position vectors from the origin of the right and left wing planform frames to the centers of pressure of the blade elements at a spanwise location

r expressed in the body frame. The centers of pressure of each blade element are assumed to be at the center of each element. Therefore,

$$\boldsymbol{r}_{p_{\mathrm{RW}}}^{\mathrm{RW}P} = \begin{bmatrix} -\frac{c(r)}{2} \\ r \\ 0 \end{bmatrix}; \qquad \boldsymbol{r}_{p_{\mathrm{LW}}}^{\mathrm{LW}P} = \begin{bmatrix} -\frac{c(r)}{2} \\ r \\ 0 \end{bmatrix} \tag{16}$$

where $c(r)$ is the wing chord at a spanwise location r. These vectors can be transformed into body frame coordinates using

$$\begin{aligned} \boldsymbol{r}_{p_{\mathrm{RW}}}^{B} &= \Delta\mathbf{r}_{\mathrm{RW}}^{B} + \boldsymbol{R}_{\mathrm{RS}}^{\mathrm{RW}R}\boldsymbol{R}_{\mathrm{RW}P}^{\mathrm{RS}}\boldsymbol{r}_{p_{\mathrm{RW}}}^{\mathrm{RW}P} \\ \boldsymbol{r}_{p_{\mathrm{LW}}}^{B} &= \Delta\mathbf{r}_{\mathrm{LW}}^{B} + \boldsymbol{R}_{\mathrm{LS}}^{\mathrm{LW}R}\boldsymbol{R}_{\mathrm{LW}P}^{\mathrm{LS}}\boldsymbol{r}_{p_{\mathrm{LW}}}^{\mathrm{LW}P} \end{aligned} \tag{17}$$

Substituting Eq. (17) into Eq. (15), the expressions for the velocities due to rigid-body rotation become

$$\begin{aligned} \mathbf{v}_{R_{\mathrm{RW}}}^{\mathrm{RS}}(r) &= \boldsymbol{R}_{\mathrm{RW}R}^{\mathrm{RS}}[\boldsymbol{\omega}_b^B \times (\Delta\mathbf{r}_{\mathrm{RW}}^{B} + \boldsymbol{R}_{\mathrm{RS}}^{\mathrm{RW}R}\boldsymbol{R}_{\mathrm{RW}P}^{\mathrm{RS}}\boldsymbol{r}_{p_{\mathrm{RW}}}^{\mathrm{RW}P})] \\ \mathbf{v}_{R_{\mathrm{LW}}}^{\mathrm{LS}}(r) &= \boldsymbol{R}_{\mathrm{LW}R}^{\mathrm{LS}}[\boldsymbol{\omega}_b^B \times (\Delta\mathbf{r}_{\mathrm{LW}}^{B} + \boldsymbol{R}_{\mathrm{LS}}^{\mathrm{LW}R}\boldsymbol{R}_{\mathrm{LW}P}^{\mathrm{LS}}\boldsymbol{r}_{p_{\mathrm{LW}}}^{\mathrm{LW}P})] \end{aligned} \tag{18}$$

All of the components of the velocity are now concisely expressed in well-defined terms.

To compute the angle of attack, consider a blade element along the chord of the wing. Note that the relative wind will vary across the span of each wing. Defining the relative wind velocity frames (denoted RRWV and LRWV for right and left relative wind velocity frames, respectively), such that the x axes of the RRWV and LRWV frames are aligned with the vector formed by only considering the x and z components of $-\mathbf{v}_{\mathrm{RW}}^{\mathrm{RS}}$ and $-\mathbf{v}_{\mathrm{LW}}^{\mathrm{LS}}$ (denote these vectors by $\mathbf{v}_{\infty_{\mathrm{RW}}}$ and $\mathbf{v}_{\infty_{\mathrm{LW}}}$), the y axes of the RRWV and LRWV frames are along the right and left spar frame's positive y axes, and the z axes complete the right-hand rule. This implies that the rotations from/to the RRWV and LRWV frames to/from the spar frames are only one rotation about the y axes. Furthermore, define the drag force as always positive and along the RRWV and LRWV x axes. Therefore, the aerodynamic (blade element) force vector expressed in the RRWV and LRWV frames will always have a positive x component due to drag, a zero y component, and either a positive or negative z component due to lift.

Define the angles

$$\alpha_{v_{\mathrm{RW}}} = \operatorname{atan}(v_{\mathrm{RW}_z}^{\mathrm{RS}}, v_{\mathrm{RW}_x}^{\mathrm{RS}}); \qquad \alpha_{v_{\mathrm{LW}}} = \operatorname{atan}(v_{\mathrm{LW}_z}^{\mathrm{LS}}, v_{\mathrm{LW}_x}^{\mathrm{LS}}) \tag{19}$$

The rotation matrices from the spar frames to the RRWV and LRWV frames are

$$\begin{aligned} \boldsymbol{R}_{\mathrm{RS}}^{\mathrm{RRWV}} &= \begin{bmatrix} \cos\alpha_{v_{\mathrm{RW}}} & 0 & \sin\alpha_{v_{\mathrm{RW}}} \\ 0 & 1 & 0 \\ -\sin\alpha_{v_{\mathrm{RW}}} & 0 & \cos\alpha_{v_{\mathrm{RW}}} \end{bmatrix}; \\ \boldsymbol{R}_{\mathrm{LS}}^{\mathrm{LRWV}} &= \begin{bmatrix} \cos\alpha_{v_{\mathrm{LW}}} & 0 & \sin\alpha_{v_{\mathrm{LW}}} \\ 0 & 1 & 0 \\ -\sin\alpha_{v_{\mathrm{LW}}} & 0 & \cos\alpha_{v_{\mathrm{LW}}} \end{bmatrix} \end{aligned} \tag{20}$$

The angles of attack, α_{RW} and α_{LW}, are defined as the absolute value of the smallest angle from the x axes of the RRWV and LRWV frames to the wing chords (blade element). Figure 4 shows the aerodynamic forces, expressed in a relative wind velocity frame, for four cases of interest. Note that the expressions in Fig. 4, although written for the right wing, are also valid for the left wing. The angles $\alpha_{w_{\mathrm{RW}}}$ and $\alpha_{w_{\mathrm{LW}}}$ are defined as the angles between the positive x axis of the spar frame and the wing chord (or blade element) and are set by the passive-wing rotation joints.

With the wing velocities and angles of attack calculated, the blade-element forces, expressed in the RRWV and LRWV frames, are

$$\begin{aligned} \mathrm{d}L_{\mathrm{RW}} &= \frac{\rho}{2}\|[1 \quad 0 \quad 0]\ \boldsymbol{R}_{\mathrm{RS}}^{\mathrm{RRWV}}\ \mathbf{v}_{\infty_{\mathrm{RW}}}\|^2 C_L(\alpha_{\mathrm{RW}})c(r)\,\mathrm{d}r \\ \mathrm{d}D_{\mathrm{RW}} &= \frac{\rho}{2}\|[1 \quad 0 \quad 0]\ \boldsymbol{R}_{\mathrm{RS}}^{\mathrm{RRWV}}\ \mathbf{v}_{\infty_{\mathrm{RW}}}\|^2 C_D(\alpha_{\mathrm{RW}})c(r)\,\mathrm{d}r \\ \mathrm{d}L_{\mathrm{LW}} &= \frac{\rho}{2}\|[1 \quad 0 \quad 0]\ \boldsymbol{R}_{\mathrm{LS}}^{\mathrm{LRWV}}\ \mathbf{v}_{\infty_{\mathrm{LW}}}\|^2 C_L(\alpha_{\mathrm{LW}})c(r)\,\mathrm{d}r \\ \mathrm{d}D_{\mathrm{LW}} &= \frac{\rho}{2}\|[1 \quad 0 \quad 0]\ \boldsymbol{R}_{\mathrm{LS}}^{\mathrm{LRWV}}\ \mathbf{v}_{\infty_{\mathrm{LW}}}\|^2 C_D(\alpha_{\mathrm{LW}})c(r)\,\mathrm{d}r \end{aligned} \tag{21}$$

The lift and drag coefficients use the Sane and Dickinson [5] expressions

$$\begin{aligned} C_{L_{\mathrm{RW}}}(\alpha_{\mathrm{RW}}) &= 0.225 + 1.58\sin(2.13\alpha_{\mathrm{RW}} - 7.2) \\ C_{D_{\mathrm{RW}}}(\alpha_{\mathrm{RW}}) &= 1.92 - 1.55\cos(2.04\alpha_{\mathrm{RW}} - 9.82) \\ C_{L_{\mathrm{LW}}}(\alpha_{\mathrm{LW}}) &= 0.225 + 1.58\sin(2.13\alpha_{\mathrm{LW}} - 7.2) \\ C_{D_{\mathrm{LW}}}(\alpha_{\mathrm{LW}}) &= 1.92 - 1.55\cos(2.04\alpha_{\mathrm{LW}} - 9.82) \end{aligned} \tag{22}$$

where α_{RW} and α_{LW} are in degrees. The differential lift and drag contributions in the spar frame are

$$\begin{aligned} \mathrm{d}\boldsymbol{F}_{\mathrm{aero}_{\mathrm{RW}}}^{\mathrm{RS}}(r) &= \boldsymbol{R}_{\mathrm{RRWV}}^{\mathrm{RS}}\,\mathrm{d}\boldsymbol{F}_{\mathrm{aero}_{\mathrm{RW}}}^{\mathrm{RRWV}}(r) \\ \mathrm{d}\boldsymbol{F}_{\mathrm{aero}_{\mathrm{LW}}}^{\mathrm{LS}}(r) &= \boldsymbol{R}_{\mathrm{LRWV}}^{\mathrm{LS}}\,\mathrm{d}\boldsymbol{F}_{\mathrm{aero}_{\mathrm{LW}}}^{\mathrm{LRWV}}(r) \end{aligned} \tag{23}$$

where $\mathrm{d}\mathbf{F}_{\mathrm{aero}_{\mathrm{RW}}}^{\mathrm{RRWV}}(r)$ and $\mathrm{d}\mathbf{F}_{\mathrm{aero}_{\mathrm{LW}}}^{\mathrm{LRWV}}(r)$ are obtained as one of the cases in Fig. 4. The differential moments due to the aerodynamic forces are

$$\begin{aligned} \mathrm{d}\boldsymbol{M}_{\mathrm{aero}_{\mathrm{RW}}}^{B}(r) &= \mathbf{r}_{p\mathrm{RW}}^{B}(r) \times [\boldsymbol{R}_{\mathrm{RS}}^{B}\boldsymbol{R}_{\mathrm{RRWV}}^{\mathrm{RS}}\,\mathrm{d}\boldsymbol{F}_{\mathrm{aero}_{\mathrm{RW}}}^{\mathrm{RRWV}}(r)] \\ \mathrm{d}\boldsymbol{M}_{\mathrm{aero}_{\mathrm{LW}}}^{B}(r) &= \mathbf{r}_{p\mathrm{LW}}^{B}(r) \times [\boldsymbol{R}_{\mathrm{LS}}^{B}\boldsymbol{R}_{\mathrm{LRWV}}^{\mathrm{LS}}\,\mathrm{d}\boldsymbol{F}_{\mathrm{aero}_{\mathrm{LW}}}^{\mathrm{LRWV}}(r)] \end{aligned} \tag{24}$$

Note that the rotation matrices $\boldsymbol{R}_{\mathrm{RRWV}}^{\mathrm{RS}}$ and $\boldsymbol{R}_{\mathrm{LRWV}}^{\mathrm{LS}}$ are functions of the spanwise location r. The differential forces and moments are integrated along both the right and left spars in order to compute the total aerodynamic forces and moments due to each wing. These total instantaneous aerodynamic forces and moments drive the 6-DOF equations of motion. The equations of motion used in this work are the same as those used by Doman et al. [12].

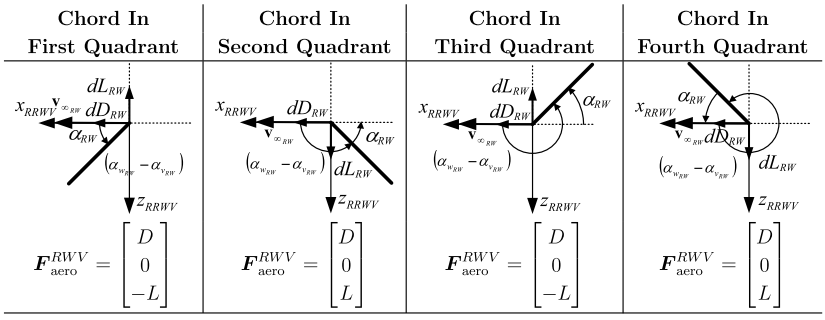

Fig. 4 The aerodynamic forces and angles of attack for a blade element in each of the quadrants of a relative wind velocity frame. These figures are drawn with right wing variables but also hold for left wing variables.

IV. Cycle-Averaged Aerodynamic Forces and Moments

This section focuses on the calculation of parameters for use in a flapping-wing vehicle control law. The parameters that are available to be manipulated for control are ω_{LW}, ω_{RW}, δ_{LW}, δ_{RW}, η_{LW}, and η_{RW}, which are the fundamental frequencies, split-cycle parameters, and wing biases for the left and right wings, respectively. It will be shown that feedback control laws based on cycle-averaged forces and moments will allow the vehicle to track desired angular and spatial positions in a mean sense; however, because of the true periodic nature of the aerodynamic forces, the vehicle will exhibit limit-cycle behavior in a neighborhood about the mean position.

In this section, expressions for the cycle-averaged forces and moments are derived. Without loss of generality, the time at the beginning of each wingbeat cycle is taken to be zero. Since the introduction of the split-cycle parameter changes the frequency of the cosine wave when $(\omega - \delta)t = \pi$ in each cycle, and because the downstroke is split into two parts, it is convenient to split the integrals (used to evaluate the cycle-averaged forces and moments) as follows:

$$\bar{G} = \frac{\omega}{2\pi}\left\{\int_0^{\pi/(\omega-\delta)} G[\phi_u(t)]\,\mathrm{d}t + \int_{\pi/(\omega-\delta)}^{[\pi(3\omega-2\delta)]/[2\omega(\omega-\delta)]} G[\phi_d(t)]\,\mathrm{d}t + \int_{[\pi(3\omega-2\delta)]/[2\omega(\omega-\delta)]}^{2\pi/\omega} G[\phi_d(t)]\,\mathrm{d}t\right\} \tag{25}$$

where the downstroke is split into first-half and second-half parts. Note that $G(\cdot)$ in Eq. (25) is a generalized force that represents either a force or moment. To calculate the cycle-averaged forces and moments, it will be necessary to evaluate numerous integrals. Many have no indefinite integral solutions. For example, many of the integrands will be of the form $\cos(\cos\omega t)$ or $\sin(\cos\omega t)$ because of the transformations from wing planform axes to body axes and the fact that the motion of each wing in the stroke plane is sinusoidal. Fortunately, definite integrals involving such functions exist over the intervals of interest for the present problem and can be derived from results presented in Gradshteyn and Ryzhik [35]. These integrals are provided by Oppenheimer et al. [36].

As an example cycle-average computation, the x-body axis force is calculated by substituting the expression for the instantaneous x-body force from Table 1 into Eq. (25) to yield

$$\bar{X}^B_{\mathrm{RW}} = \frac{\omega_{\mathrm{RW}}}{2\pi}\left[\int_0^{\pi/(\omega_{\mathrm{RW}}-\delta_{\mathrm{RW}})} L_{u_{\mathrm{RW}}}(t)\,\mathrm{d}t + \int_{\pi/(\omega_{\mathrm{RW}}-\delta_{\mathrm{RW}})}^{[\pi(3\omega_{\mathrm{RW}}-2\delta_{\mathrm{RW}})]/[2\omega_{\mathrm{RW}}(\omega_{\mathrm{RW}}-\delta_{\mathrm{RW}})]} L_{d_{\mathrm{RW}}}(t)\,\mathrm{d}t + \int_{[\pi(3\omega_{\mathrm{RW}}-2\delta_{\mathrm{RW}})]/[2\omega_{\mathrm{RW}}(\omega_{\mathrm{RW}}-\delta_{\mathrm{RW}})]}^{2\pi/\omega_{\mathrm{RW}}} L_{d_{\mathrm{RW}}}(t)\,\mathrm{d}t\right] \tag{26}$$

Performing the integrations yields

$$\bar{X}^B_{\mathrm{RW}} = \frac{k_L\omega_{\mathrm{RW}}}{4}\left[(\omega_{\mathrm{RW}} - \delta_{\mathrm{RW}}) + \frac{(\omega_{\mathrm{RW}} + \sigma_{\mathrm{RW}})}{2}\{1 + (1 + \Delta A_{\mathrm{RW}})^2\}\right] \tag{27}$$

Following a similar procedure for the left wing, it can be shown that

$$\bar{X}^B_{\mathrm{LW}} = \frac{k_L\omega_{\mathrm{LW}}}{4}\left[(\omega_{\mathrm{LW}} - \delta_{\mathrm{LW}}) + \frac{(\omega_{\mathrm{LW}} + \sigma_{\mathrm{LW}})}{2}\{1 + (1 + \Delta A_{\mathrm{LW}})^2\}\right] \tag{28}$$

Note that both $\bar{X}^B_{\mathrm{RW}}$ and $\bar{X}^B_{\mathrm{LW}}$ are positive quantities. At a hover condition, where the x-body axis is normal to the surface of the Earth, the forces produced by both wings act to counter the weight of the vehicle. Also, from Eqs. (28) and (29), it can be seen that wing bias has a secondary effect on the vertical force produced and only appears in the ΔA_{RW} and ΔA_{LW} terms. In practice, it is expected that $\Delta A_{\mathrm{RW}} \ll 1$ and $\Delta A_{\mathrm{LW}} \ll 1$; thus, minor changes to vertical force will be experienced by a nonzero wing bias. Recall, from Doman et al. [12], that when no wing bias is used, $\bar{X}^B_{\mathrm{RW}} = (k_L\omega_{\mathrm{RW}}/4)(2\omega_{\mathrm{RW}} - \delta_{\mathrm{RW}} + \sigma_{\mathrm{RW}})$, and similarly for the left wing. Comparing this previous result with the expression in Eq. (27) shows that the increase in x-body axis force resulting from the introduction of a wing bias is given by

$$\frac{k_L\omega_{\mathrm{RW}}(\omega_{\mathrm{RW}} + \sigma_{\mathrm{RW}})}{8}\{2\Delta A_{\mathrm{RW}} + \Delta A^2_{\mathrm{RW}}\}$$

and similarly for the left wing. Calculation of the remaining cycle-averaged forces and moments can be found in Oppenheimer et al. [36].

V. Control Derivatives

The parameters used to control the aerodynamic forces and moments are the fundamental wingbeat frequencies, ω_{RW} and ω_{LW}, the split-cycle parameters, δ_{RW} and δ_{LW}, and the wing biases, η_{RW} and η_{LW}. For controllability analysis and control synthesis, the sensitivity of each cycle-averaged force and moment to each control input parameter must be determined. The forces and moments are, in general, functions of the control input parameters as well as the past values of η_{RW} and η_{LW}, because $\Delta A_i = \eta_i - \eta_{i-1} = \eta - \eta_{-1}$. Note that the subscript i notation has been removed, and it should be understood that $\eta \triangleq \eta_i$ (the current value of wing bias) and $\eta_{-1} \triangleq \eta_{i-1}$ (the one cycle past value of wing bias). Hence, the cycle-averaged forces and moments are sensitive to changes in η_{-1}, although η_{-1} is not considered a control input because it is a fixed value that was calculated one full wingbeat cycle before calculating η. Thus, sensitivities of cycle-averaged forces and moments to changes in η_{-1} are also calculated. Let $\bar{G}_i$, $i = 1, 2, \ldots, 6$, be a generalized cycle-averaged force. Then, a first-order approximation of $\bar{G}_i$ can be expressed as

$$\bar{G}_i = \bar{G}_o + \Delta\bar{G}_i \tag{29}$$

where $\bar{G}_o$ is the generalized cycle-averaged force necessary to hover (trim) the vehicle, and

$$\Delta\bar{G}_i = \frac{\partial\bar{G}_i}{\partial\omega_{\mathrm{RW}}}\Delta\omega_{\mathrm{RW}} + \frac{\partial\bar{G}_i}{\partial\omega_{\mathrm{LW}}}\Delta\omega_{\mathrm{LW}} + \frac{\partial\bar{G}_i}{\partial\delta_{\mathrm{RW}}}\delta_{\mathrm{RW}} + \frac{\partial\bar{G}_i}{\partial\delta_{\mathrm{LW}}}\delta_{\mathrm{LW}} + \frac{\partial\bar{G}_i}{\partial\eta_{\mathrm{RW}}}\eta_{\mathrm{RW}} + \frac{\partial\bar{G}_i}{\partial\eta_{\mathrm{LW}}}\eta_{\mathrm{LW}} + \frac{\partial\bar{G}_i}{\partial\eta_{\mathrm{RW}-1}}\eta_{\mathrm{RW}-1} + \frac{\partial\bar{G}_i}{\partial\eta_{\mathrm{LW}-1}}\eta_{\mathrm{LW}-1} \tag{30}$$

Note that, in Eq. (30), increments to fundamental frequency are used, since nonzero fundamental frequencies are required to hover the vehicle. A feedback controller will generate a vector of desired cycle-averaged forces and moments, with each scalar quantity being denoted by $\Delta\bar{G}_{i_{\mathrm{des}}}$. The control inputs should then be chosen so as to generate $\Delta\bar{G}_{i_{\mathrm{des}}}$. Near hover, the control allocation problem is to find the control inputs such that the following equations are satisfied:

$$\Delta\bar{G}_{i_{\mathrm{des}}} = \left.\frac{\partial\bar{G}_i}{\partial\omega_{\mathrm{RW}}}\right|_{\mathrm{hover}}\Delta\omega_{\mathrm{RW}} + \left.\frac{\partial\bar{G}_i}{\partial\omega_{\mathrm{LW}}}\right|_{\mathrm{hover}}\Delta\omega_{\mathrm{LW}} + \left.\frac{\partial\bar{G}_i}{\partial\delta_{\mathrm{RW}}}\right|_{\mathrm{hover}}\delta_{\mathrm{RW}} + \left.\frac{\partial\bar{G}_i}{\partial\delta_{\mathrm{LW}}}\right|_{\mathrm{hover}}\delta_{\mathrm{LW}} + \left.\frac{\partial\bar{G}_i}{\partial\eta_{\mathrm{RW}}}\right|_{\mathrm{hover}}\eta_{\mathrm{RW}} + \left.\frac{\partial\bar{G}_i}{\partial\eta_{\mathrm{LW}}}\right|_{\mathrm{hover}}\eta_{\mathrm{LW}} + \left.\frac{\partial\bar{G}_i}{\partial\eta_{\mathrm{RW}-1}}\right|_{\mathrm{hover}}\eta_{\mathrm{RW}-1} + \left.\frac{\partial\bar{G}_i}{\partial\eta_{\mathrm{LW}-1}}\right|_{\mathrm{hover}}\eta_{\mathrm{LW}-1} \tag{31}$$

where $i = 1, 2, \ldots, 6$. Expressions for the cycle-averaged forces and moments are given by Oppenheimer et al. [36]. For brevity, only one set of control derivatives are explicitly shown here, and the remaining

are given by Doman et al. [37]. The goal of the following section is to compute the partial derivatives in Eq. (30). Following this, the partial derivatives are evaluated at the hover operating point to provide the entries in Eq. (31).

To compute the sensitivity of the x-body axis force to changes in the control parameters and past values of wing biases, partial derivatives of Eq. (27), with respect to each of these variables, are computed. The results are

$$\frac{\partial \bar{F}^B_{x\mathrm{RW}}}{\partial \delta_{\mathrm{RW}}} = \frac{k_L}{4}\left\{-\omega_{\mathrm{RW}} + \frac{\omega^3_{\mathrm{RW}}}{2(\omega_{\mathrm{RW}} - 2\delta_{\mathrm{RW}})^2}[1 + (1 + \Delta A_{\mathrm{RW}})^2]\right\} \tag{32}$$

$$\frac{\partial \bar{F}^B_{x\mathrm{RW}}}{\partial \omega_{\mathrm{RW}}} = \frac{k_L}{4}\left\{(2\omega_{\mathrm{RW}} - \delta_{\mathrm{RW}}) + \left(\frac{2\omega^3_{\mathrm{RW}} - 7\delta_{\mathrm{RW}}\omega^2_{\mathrm{RW}} + 4\omega_{\mathrm{RW}}\delta^2_{\mathrm{RW}}}{2(\omega_{\mathrm{RW}} - 2\delta_{\mathrm{RW}})^2}\right)[1 + (1 + \Delta A_{\mathrm{RW}})^2]\right\} \tag{33}$$

For the x-body axis force sensitivity with respect to η_{RW}, recall that ΔA_{RW} is a function of η_{RW}. Therefore,

$$\frac{\partial \bar{F}^B_{x\mathrm{RW}}}{\partial \eta_{\mathrm{RW}}} = \frac{k_L \omega_{\mathrm{RW}}(\omega_{\mathrm{RW}} + \sigma_{\mathrm{RW}})}{4}(1 + \Delta A_{\mathrm{RW}})\frac{\partial \Delta A_{\mathrm{RW}}}{\partial \eta_{\mathrm{RW}}} \tag{34}$$

$$\frac{\partial \bar{F}^B_{x\mathrm{RW}}}{\partial \eta_{\mathrm{RW}-1}} = \frac{k_L \omega_{\mathrm{RW}}(\omega_{\mathrm{RW}} + \sigma_{\mathrm{RW}})}{4}(1 + \Delta A_{\mathrm{RW}})\frac{\partial \Delta A_{\mathrm{RW}}}{\partial \eta_{\mathrm{RW}-1}} \tag{35}$$

Left wing expressions are of the same form as the right wing [37].

VI. Aerodynamic Control Derivatives About Hover

The control of this vehicle in the vicinity of hover is of considerable interest. Therefore, the control derivatives are evaluated at the hover condition, where $\omega_{\mathrm{RW}} = \omega_{\mathrm{LW}} = \omega_o$, $\delta_{\mathrm{RW}} = \delta_{\mathrm{LW}} = 0$, $\eta_{\mathrm{RW}} = \eta_{\mathrm{LW}} = 0$, and $\Delta A_{\mathrm{RW}} = \Delta A_{\mathrm{LW}} = 0$. Note that ω_o is the frequency at which the cycle-averaged lift is equal to the weight of the vehicle, also called the hover frequency [12]. Additionally, it is assumed that the vehicle has been designed such that the nominal center of gravity of the vehicle and wing root hinges are aligned on the z-body axis; therefore, $\Delta z^B_{\mathrm{RW}} = \Delta z^B_{\mathrm{LW}} = 0$. When the nominal center of gravity and wing root hinges are not aligned, a nonzero cycle-averaged pitching moment is produced, even if the wing bias terms are zero, and hover is not achieved. Recall that $\Delta A = \eta - \eta_{-1}$; therefore, $\partial \Delta A/\partial \eta = 1$ and $\partial \Delta A/\partial \eta_{-1} = -1$. All control derivatives, computed about hover, are shown in the following sections.

A. Cycle-Averaged *X*-Body Axis Force Control Derivatives About Hover

$$\left.\frac{\partial \bar{F}^B_{x\mathrm{RW}}}{\partial \delta_{\mathrm{RW}}}\right|_{\mathrm{hover}} = \left.\frac{\partial \bar{F}^B_{x\mathrm{LW}}}{\partial \delta_{\mathrm{LW}}}\right|_{\mathrm{hover}} = 0 \tag{36}$$

$$\left.\frac{\partial \bar{F}^B_{x\mathrm{RW}}}{\partial \omega_{\mathrm{RW}}}\right|_{\mathrm{hover}} = \left.\frac{\partial \bar{F}^B_{x\mathrm{LW}}}{\partial \omega_{\mathrm{LW}}}\right|_{\mathrm{hover}} = k_L \omega_o \tag{37}$$

$$\left.\frac{\partial \bar{F}^B_{x\mathrm{RW}}}{\partial \eta_{\mathrm{RW}}}\right|_{\mathrm{hover}} = -\left.\frac{\partial \bar{F}^B_{x\mathrm{RW}}}{\partial \eta_{\mathrm{RW}-1}}\right|_{\mathrm{hover}} = \left.\frac{\partial \bar{F}^B_{x\mathrm{LW}}}{\partial \eta_{\mathrm{LW}}}\right|_{\mathrm{hover}} = -\left.\frac{\partial \bar{F}^B_{x\mathrm{LW}}}{\partial \eta_{\mathrm{LW}-1}}\right|_{\mathrm{hover}} = \frac{k_L \omega_o^2}{4} \tag{38}$$

B. Cycle-Averaged *Y*-Body Axis Force Control Derivatives About Hover

$$\left.\frac{\partial \bar{F}^B_{y\mathrm{RW}}}{\partial \delta_{\mathrm{RW}}}\right|_{\mathrm{hover}} = \left.\frac{\partial \bar{F}^B_{y\mathrm{LW}}}{\partial \delta_{\mathrm{LW}}}\right|_{\mathrm{hover}} = \left.\frac{\partial \bar{F}^B_{y\mathrm{RW}}}{\partial \omega_{\mathrm{RW}}}\right|_{\mathrm{hover}} = \left.\frac{\partial \bar{F}^B_{y\mathrm{LW}}}{\partial \omega_{\mathrm{LW}}}\right|_{\mathrm{hover}} = 0 \tag{39}$$

$$\left.\frac{\partial \bar{F}^B_{y\mathrm{RW}}}{\partial \eta_{\mathrm{RW}}}\right|_{\mathrm{hover}} = \left.\frac{-\partial \bar{F}^B_{y\mathrm{RW}}}{\partial \eta_{\mathrm{RW}-1}}\right|_{\mathrm{hover}} = \frac{k_D \omega_o^2}{4}\left[H_1(1) + \left.\frac{\partial H_1(1 + \Delta A_{\mathrm{RW}})}{\partial(1 + \Delta A_{\mathrm{RW}})}\right|_{\mathrm{hover}}\right] \tag{40}$$

$$\left.\frac{\partial \bar{F}^B_{y\mathrm{LW}}}{\partial \eta_{\mathrm{LW}}}\right|_{\mathrm{hover}} = -\left.\frac{\partial \bar{F}^B_{y\mathrm{LW}}}{\partial \eta_{\mathrm{LW}-1}}\right|_{\mathrm{hover}} = -\frac{k_D \omega_o^2}{4}\left[H_1(1) + \left.\frac{\partial H_1(1 + \Delta A_{\mathrm{LW}})}{\partial(1 + \Delta A_{\mathrm{LW}})}\right|_{\mathrm{hover}}\right] \tag{41}$$

Note that when wing bias is included in the forcing function, a side force can be generated. This was not possible with SCCPFM alone. In Eq. (41), $H_1(\cdot)$ is a Struve function [35].

C. Cycle-Averaged *Z*-Body Axis Force Control Derivatives About Hover

$$\left.\frac{\partial \bar{F}^B_{z\mathrm{RW}}}{\partial \delta_{\mathrm{RW}}}\right|_{\mathrm{hover}} = \left.\frac{\partial \bar{F}^B_{z\mathrm{LW}}}{\partial \delta_{\mathrm{LW}}}\right|_{\mathrm{hover}} = -k_D J_1(1)\omega_o \tag{42}$$

$$\left.\frac{\partial \bar{F}^B_{z\mathrm{RW}}}{\partial \omega_{\mathrm{RW}}}\right|_{\mathrm{hover}} = \left.\frac{\partial \bar{F}^B_{z\mathrm{LW}}}{\partial \omega_{\mathrm{LW}}}\right|_{\mathrm{hover}} = 0 \tag{43}$$

$$\left.\frac{\partial \bar{F}^B_{z\mathrm{RW}}}{\partial \eta_{\mathrm{RW}}}\right|_{\mathrm{hover}} = -\left.\frac{\partial \bar{F}^B_{z\mathrm{RW}}}{\partial \eta_{\mathrm{RW}-1}}\right|_{\mathrm{hover}} = -\frac{k_D \omega_o^2}{4}\left[J_1(1) + \left.\frac{\partial J_1(1 + \Delta A_{\mathrm{RW}})}{\partial(1 + \Delta A_{\mathrm{RW}})}\right|_{\mathrm{hover}}\right] \tag{44}$$

$$\left.\frac{\partial \bar{F}^B_{z\mathrm{LW}}}{\partial \eta_{\mathrm{LW}}}\right|_{\mathrm{hover}} = -\left.\frac{\partial \bar{F}^B_{z\mathrm{LW}}}{\partial \eta_{\mathrm{LW}-1}}\right|_{\mathrm{hover}} = -\frac{k_D \omega_o^2}{4}\left[J_1(1) + \left.\frac{\partial J_1(1 + \Delta A_{\mathrm{LW}})}{\partial(1 + \Delta A_{\mathrm{LW}})}\right|_{\mathrm{hover}}\right] \tag{45}$$

where $J_1(\cdot)$ is a Bessel function of the first kind.

D. Cycle-Averaged Rolling Moment Control Derivatives About Hover

$$\left.\frac{\partial \bar{M}^B_{x\mathrm{RW}}}{\partial \delta_{\mathrm{RW}}}\right|_{\mathrm{hover}} = -\left.\frac{\partial \bar{M}^B_{x\mathrm{LW}}}{\partial \delta_{\mathrm{LW}}}\right|_{\mathrm{hover}} = -\frac{k_D \omega_o}{2}[y^{\mathrm{WP}}_{\mathrm{cp}} + wJ_1(1)] \tag{46}$$

$$\left.\frac{\partial \bar{M}^B_{x\mathrm{RW}}}{\partial \omega_{\mathrm{RW}}}\right|_{\mathrm{hover}} = \left.\frac{\partial \bar{M}^B_{x\mathrm{LW}}}{\partial \omega_{\mathrm{LW}}}\right|_{\mathrm{hover}} = 0 \tag{47}$$

$$\left.\frac{\partial \bar{M}^B_{x\mathrm{RW}}}{\partial \eta_{\mathrm{RW}}}\right|_{\mathrm{hover}} = -\left.\frac{\partial \bar{M}^B_{x\mathrm{RW}}}{\partial \eta_{\mathrm{RW}-1}}\right|_{\mathrm{hover}} = -\frac{k_D \omega_o^2}{8}\left\{2y^{\mathrm{WP}}_{\mathrm{cp}} + w\left[J_1(1) + \left.\frac{\partial J_1(1 + \Delta A_{\mathrm{RW}})}{\partial(1 + \Delta A_{\mathrm{RW}})}\right|_{\mathrm{hover}}\right]\right\} \tag{48}$$

$$\left.\frac{\partial \bar{M}^B_{x\mathrm{LW}}}{\partial \eta_{\mathrm{LW}}}\right|_{\mathrm{hover}} = \left.\frac{-\partial \bar{M}^B_{x\mathrm{LW}}}{\partial \eta_{\mathrm{LW}-1}}\right|_{\mathrm{hover}} = \frac{k_D \omega_o^2}{8}\left\{2y_{\mathrm{cp}}^{\mathrm{WP}} + w\left[J_1(1) + \left.\frac{\partial J_1(1+\Delta A_{\mathrm{LW}})}{\partial(1+\Delta A_{\mathrm{LW}})}\right|_{\mathrm{hover}}\right]\right\} \tag{49}$$

E. Cycle-Averaged Pitching-Moment Control Derivatives About Hover

$$\left.\frac{\partial \bar{M}^B_{y\mathrm{RW}}}{\partial \delta_{\mathrm{RW}}}\right|_{\mathrm{hover}} = J_1(1)\omega_o(\cos\alpha x_{\mathrm{cp}}^{\mathrm{WP}} k_L + \{\sin\alpha x_{\mathrm{cp}}^{\mathrm{WP}} + \Delta x^B_{\mathrm{RW}}\}k_D) \tag{50}$$

$$\left.\frac{\partial \bar{M}^B_{y\mathrm{LW}}}{\partial \delta_{\mathrm{LW}}}\right|_{\mathrm{hover}} = J_1(1)\omega_o(\cos\alpha x_{\mathrm{cp}}^{\mathrm{WP}} k_L + \{\sin\alpha x_{\mathrm{cp}}^{\mathrm{WP}} + \Delta x^B_{\mathrm{LW}}\}k_D) \tag{51}$$

$$\left.\frac{\partial \bar{M}^B_{y\mathrm{RW}}}{\partial \omega_{\mathrm{RW}}}\right|_{\mathrm{hover}} = \left.\frac{\partial \bar{M}^B_{y\mathrm{LW}}}{\partial \omega_{\mathrm{LW}}}\right|_{\mathrm{hover}} = 0 \tag{52}$$

$$\left.\frac{\partial \bar{M}^B_{y\mathrm{RW}}}{\partial \eta_{\mathrm{RW}}}\right|_{\mathrm{hover}} = \omega_o^2 y_{\mathrm{cp}}^{\mathrm{WP}} k_L J_1(1) + \frac{\omega_o^2}{4}\left[\left(\cos\alpha x_{\mathrm{cp}}^{\mathrm{WP}} k_L + \{\sin\alpha x_{\mathrm{cp}}^{\mathrm{WP}} + \Delta x^B_{\mathrm{RW}}\}k_D\right)\left\{J_1(1) + \left.\frac{\partial J_1(1+\Delta A_{\mathrm{RW}})}{\partial(1+\Delta A_{\mathrm{RW}})}\right|_{\mathrm{hover}}\right\} + y_{\mathrm{cp}}^{\mathrm{WP}} k_L\left\{H_1(1) + \left.\frac{\partial H_1(1+\Delta A_{\mathrm{RW}})}{\partial(1+\Delta A_{\mathrm{RW}})}\right|_{\mathrm{hover}}\right\}\right] \tag{53}$$

$$\left.\frac{\partial \bar{M}^B_{y\mathrm{LW}}}{\partial \eta_{\mathrm{LW}}}\right|_{\mathrm{hover}} = \omega_o^2 y_{\mathrm{cp}}^{\mathrm{WP}} k_L J_1(1) + \frac{\omega_o^2}{4}\left[\left(\cos\alpha x_{\mathrm{cp}}^{\mathrm{WP}} k_L + \{\sin\alpha x_{\mathrm{cp}}^{\mathrm{WP}} + \Delta x^B_{\mathrm{LW}}\}k_D\right)\left\{J_1(1) + \left.\frac{\partial J_1(1+\Delta A_{\mathrm{LW}})}{\partial(1+\Delta A_{\mathrm{LW}})}\right|_{\mathrm{hover}}\right\} + y_{\mathrm{cp}}^{\mathrm{WP}} k_L\left\{H_1(1) + \left.\frac{\partial H_1(1+\Delta A_{\mathrm{LW}})}{\partial(1+\Delta A_{\mathrm{LW}})}\right|_{\mathrm{hover}}\right\}\right] \tag{54}$$

$$\left.\frac{\partial \bar{M}^B_{y\mathrm{RW}}}{\partial \eta_{\mathrm{RW}-1}}\right|_{\mathrm{hover}} = \frac{\omega_o^2}{4}\left[\left(\cos\alpha x_{\mathrm{cp}}^{\mathrm{WP}} k_L + \{\sin\alpha x_{\mathrm{cp}}^{\mathrm{WP}} + \Delta x^B_{\mathrm{RW}}\}k_D\right) \times \left\{-J_1(1) - \left.\frac{\partial J_1(1+\Delta A_{\mathrm{RW}})}{\partial(1+\Delta A_{\mathrm{RW}})}\right|_{\mathrm{hover}}\right\} + y_{\mathrm{cp}}^{\mathrm{WP}} k_L\left\{-H_1(1) - \left.\frac{\partial H_1(1+\Delta A_{\mathrm{RW}})}{\partial(1+\Delta A_{\mathrm{RW}})}\right|_{\mathrm{hover}}\right\}\right] \tag{55}$$

$$\left.\frac{\partial \bar{M}^B_{y\mathrm{LW}}}{\partial \eta_{\mathrm{LW}-1}}\right|_{\mathrm{hover}} = \frac{\omega_o^2}{4}\left[\left(\cos\alpha x_{\mathrm{cp}}^{\mathrm{WP}} k_L + \{\sin\alpha x_{\mathrm{cp}}^{\mathrm{WP}} + \Delta x^B_{\mathrm{LW}}\}k_D\right) \times \left\{-J_1(1) - \left.\frac{\partial J_1(1+\Delta A_{\mathrm{LW}})}{\partial(1+\Delta A_{\mathrm{LW}})}\right|_{\mathrm{hover}}\right\} + y_{\mathrm{cp}}^{\mathrm{WP}} k_L\left\{-H_1(1) - \left.\frac{\partial H_1(1+\Delta A_{\mathrm{LW}})}{\partial(1+\Delta A_{\mathrm{LW}})}\right|_{\mathrm{hover}}\right\}\right] \tag{56}$$

F. Cycle-Averaged Yawing-Moment Control Derivatives About Hover

$$\left.\frac{\partial \bar{M}^B_{z\mathrm{RW}}}{\partial \delta_{\mathrm{RW}}}\right|_{\mathrm{hover}} = \left.\frac{\partial \bar{M}^B_{z\mathrm{LW}}}{\partial \delta_{\mathrm{LW}}}\right|_{\mathrm{hover}} = 0 \tag{57}$$

$$\left.\frac{\partial \bar{M}^B_{z\mathrm{RW}}}{\partial \omega_{\mathrm{RW}}}\right|_{\mathrm{hover}} = -\left.\frac{\partial \bar{M}^B_{z\mathrm{LW}}}{\partial \omega_{\mathrm{LW}}}\right|_{\mathrm{hover}} = -2k_L\omega_o\left[y_{\mathrm{cp}}^{\mathrm{WP}} J_1(1) + \frac{w}{4}\right] \tag{58}$$

$$\left.\frac{\partial \bar{M}^B_{z\mathrm{RW}}}{\partial \eta_{\mathrm{RW}}}\right|_{\mathrm{hover}} = \frac{k_D\omega_o^2}{4}\left(H_1(1) + \left.\frac{\partial H_1(1+\Delta A_{\mathrm{RW}})}{\partial(1+\Delta A_{\mathrm{RW}})}\right|_{\mathrm{hover}}\right) \times (\sin\alpha x_{\mathrm{cp}}^{\mathrm{WP}} + \Delta x^B_{\mathrm{RW}}) - \frac{k_L\omega_o^2}{4}\left[-\cos\alpha x_{\mathrm{cp}}^{\mathrm{WP}}\left\{H_1(1) + \left.\frac{\partial H_1(1+\Delta A_{\mathrm{RW}})}{\partial(1+\Delta A_{\mathrm{RW}})}\right|_{\mathrm{hover}}\right\} + y_{\mathrm{cp}}^{\mathrm{WP}}\left\{J_1(1) + \left.\frac{\partial J_1(1+\Delta A_{\mathrm{RW}})}{\partial(1+\Delta A_{\mathrm{RW}})}\right|_{\mathrm{hover}}\right\} + \frac{w}{2}\right] \tag{59}$$

$$\left.\frac{\partial \bar{M}^B_{z\mathrm{LW}}}{\partial \eta_{\mathrm{LW}}}\right|_{\mathrm{hover}} = -\frac{k_D\omega_o^2}{4}\left(H_1(1) + \left.\frac{\partial H_1(1+\Delta A_{\mathrm{LW}})}{\partial(1+\Delta A_{\mathrm{LW}})}\right|_{\mathrm{hover}}\right) \times (\sin\alpha x_{\mathrm{cp}}^{\mathrm{WP}} + \Delta x^B_{\mathrm{LW}}) + \frac{k_L\omega_o^2}{4}\left[-\cos\alpha x_{\mathrm{cp}}^{\mathrm{WP}}\left\{H_1(1) + \left.\frac{\partial H_1(1+\Delta A_{\mathrm{LW}})}{\partial(1+\Delta A_{\mathrm{LW}})}\right|_{\mathrm{hover}}\right\} + y_{\mathrm{cp}}^{\mathrm{WP}}\left\{J_1(1) + \left.\frac{\partial J_1(1+\Delta A_{\mathrm{LW}})}{\partial(1+\Delta A_{\mathrm{LW}})}\right|_{\mathrm{hover}}\right\} + \frac{w}{2}\right] \tag{60}$$

$$\left.\frac{\partial \bar{M}^B_{z\mathrm{RW}}}{\partial \eta_{\mathrm{RW}-1}}\right|_{\mathrm{hover}} = -\frac{k_D\omega_o^2}{4}\left(H_1(1) + \left.\frac{\partial H_1(1+\Delta A_{\mathrm{RW}})}{\partial(1+\Delta A_{\mathrm{RW}})}\right|_{\mathrm{hover}}\right) \times (\sin\alpha x_{\mathrm{cp}}^{\mathrm{WP}} + \Delta x^B_{\mathrm{RW}}) - \frac{k_L\omega_o^2}{4}\left[\cos\alpha x_{\mathrm{cp}}^{\mathrm{WP}}\left\{H_1(1) + \left.\frac{\partial H_1(1+\Delta A_{\mathrm{RW}})}{\partial(1+\Delta A_{\mathrm{RW}})}\right|_{\mathrm{hover}}\right\} - y_{\mathrm{cp}}^{\mathrm{WP}}\left\{J_1(1) + \left.\frac{\partial J_1(1+\Delta A_{\mathrm{RW}})}{\partial(1+\Delta A_{\mathrm{RW}})}\right|_{\mathrm{hover}}\right\} - \frac{w}{2}\right] \tag{61}$$

$$\left.\frac{\partial \bar{M}^B_{z\mathrm{LW}}}{\partial \eta_{\mathrm{LW}-1}}\right|_{\mathrm{hover}} = \frac{k_D\omega_o^2}{4}\left(H_1(1) + \left.\frac{\partial H_1(1+\Delta A_{\mathrm{LW}})}{\partial(1+\Delta A_{\mathrm{LW}})}\right|_{\mathrm{hover}}\right) \times (\sin\alpha x_{\mathrm{cp}}^{\mathrm{WP}} + \Delta x^B_{\mathrm{LW}}) + \frac{k_L\omega_o^2}{4}\left[\cos\alpha x_{\mathrm{cp}}^{\mathrm{WP}}\left\{H_1(1) + \left.\frac{\partial H_1(1+\Delta A_{\mathrm{LW}})}{\partial(1+\Delta A_{\mathrm{LW}})}\right|_{\mathrm{hover}}\right\} - y_{\mathrm{cp}}^{\mathrm{WP}}\left\{J_1(1) + \left.\frac{\partial J_1(1+\Delta A_{\mathrm{LW}})}{\partial(1+\Delta A_{\mathrm{LW}})}\right|_{\mathrm{hover}}\right\} - \frac{w}{2}\right] \tag{62}$$

The derivatives of the Bessel and Struve functions are

$$\frac{\partial J_1(1+\Delta A)}{\partial(1+\Delta A)} = \frac{1}{2}[J_0(1+\Delta A) - J_2(1+\Delta A)] \tag{63}$$

$$\frac{\partial H_1(1+\Delta A)}{\partial(1+\Delta A)} = \frac{1}{2}\left[H_0(1+\Delta A) - H_2(1+\Delta A) + \frac{2(1+\Delta A)}{3\pi}\right] \tag{64}$$

G. Persistent/Nonpersistent Effects of Wing Bias

The wing bias has different effects on the forces and moments. For example, consider the x-body axis force. By examining the expressions in Eq. (38), it can be seen that the only way to produce an x-body axis force with wing bias is to have a difference between η and η_{-1}. This is because

$$\left.\frac{\partial \bar{F}^B_{x\mathrm{RW}}}{\partial \eta_{\mathrm{RW}}}\right|_{\mathrm{hover}} = -\left.\frac{\partial \bar{F}^B_{x\mathrm{RW}}}{\partial \eta_{\mathrm{RW}-1}}\right|_{\mathrm{hover}}$$

and

$$\left.\frac{\partial \bar{F}^B_{x\mathrm{LW}}}{\partial \eta_{\mathrm{LW}}}\right|_{\mathrm{hover}} = -\left.\frac{\partial \bar{F}^B_{x\mathrm{LW}}}{\partial \eta_{\mathrm{LW}-1}}\right|_{\mathrm{hover}}$$

In other words, if η is constant (that is, η has not changed from one wingbeat cycle to another), then a zero cycle-averaged x-body axis force due to wing bias is produced. In addition to the x-body axis force, this also holds for the y-body and z-body axes forces as well as the rolling and yawing moments. On the other hand, the pitching moment due to wing bias is different, in that the effects of the bias are persistent even when η does not change from one wingbeat cycle to the next. Consider Eqs. (53) and (55). The second term in Eq. (53) is equal in magnitude and opposite in sign to the expression in Eq. (55), namely, $(\partial \bar{M}^B_{y\mathrm{RW}}/\partial \eta_{\mathrm{RW}-1})|_{\mathrm{hover}}$. Hence, these terms only produce pitching moment when there is a difference between η and η_{-1}. The remaining term in $(\partial \bar{M}^B_{y\mathrm{RW}}/\partial \eta_{\mathrm{RW}})|_{\mathrm{hover}}$, $\omega_o^2 y_{\mathrm{cp}}^{\mathrm{WP}} k_L J_1(1)$, is not canceled by any terms in $(\partial \bar{M}^B_{y\mathrm{RW}}/\partial \eta_{\mathrm{RW}-1})|_{\mathrm{hover}}$. Therefore, when η is constant and $\eta \neq 0$, a persistent pitching moment is produced. Thus, wing bias produces a persistent effect on pitching moment; that is, whenever the wing bias is nonzero, a pitching moment is generated. On the other hand, wing bias has a nonpersistent effect on the remaining forces and moments, because a difference between η and η_{-1} is required to produce x-, y-, or z-body axes forces or rolling and yawing moments. A nonzero but constant wing bias over more than one full cycle produces zero x-, y-, and z-body axes forces and rolling and yawing moments. Recall that the principal reason for using the wing bias was to produce pitching moment, and it is now clear that the primary effect of wing bias serves this purpose.

H. Control Effectiveness Matrix

Using the general form of Eq. (31), writing this expression for all forces and moments and separating out the control and noncontrol parameters yields

$$\begin{bmatrix} \Delta \bar{F}^B_{x\mathrm{des}} \\ \Delta \bar{F}^B_{y\mathrm{des}} \\ \Delta \bar{F}^B_{z\mathrm{des}} \\ \Delta \bar{M}^B_{x\mathrm{des}} \\ \Delta \bar{M}^B_{y\mathrm{des}} \\ \Delta \bar{M}^B_{z\mathrm{des}} \end{bmatrix} = \mathbf{B_{A1}} \begin{bmatrix} \delta_{\mathrm{RW}} \\ \delta_{\mathrm{LW}} \\ \Delta\omega_{\mathrm{RW}} \\ \Delta\omega_{\mathrm{LW}} \\ \eta_{\mathrm{RW}} \\ \eta_{\mathrm{LW}} \end{bmatrix} + \mathbf{B_{A2}} \begin{bmatrix} -\eta_{\mathrm{RW}-1} \\ -\eta_{\mathrm{LW}-1} \end{bmatrix} \tag{65}$$

where $\mathbf{B_{A1}}$ is the control effectiveness matrix, which contains the aerodynamic control derivatives evaluated at hover, and the vector on the left side of Eq. (65) is a set of desired forces and moments, which are generated by the control law to achieve a desired maneuver. Since $\eta_{\mathrm{RW}-1}$ and $\eta_{\mathrm{LW}-1}$ are not control variables for the control input calculation from the current cycle, $\mathbf{B_{A2}}$ is not considered a control effectiveness matrix. Instead, the terms containing $\eta_{\mathrm{RW}-1}$ and $\eta_{\mathrm{LW}-1}$ simply produce a set of forces and moments that are only persistent over a single wingbeat cycle. Hence, Eq. (65) can be manipulated to give

$$\begin{bmatrix} \Delta \bar{F}^B_{x\mathrm{des}} \\ \Delta \bar{F}^B_{y\mathrm{des}} \\ \Delta \bar{F}^B_{z\mathrm{des}} \\ \Delta \bar{M}^B_{x\mathrm{des}} \\ \Delta \bar{M}^B_{y\mathrm{des}} \\ \Delta \bar{M}^B_{z\mathrm{des}} \end{bmatrix} - \mathbf{B_{A2}} \begin{bmatrix} -\eta_{\mathrm{RW}-1} \\ -\eta_{\mathrm{LW}-1} \end{bmatrix} = \mathbf{B_{A1}} \begin{bmatrix} \delta_{\mathrm{RW}} \\ \delta_{\mathrm{LW}} \\ \Delta\omega_{\mathrm{RW}} \\ \Delta\omega_{\mathrm{LW}} \\ \eta_{\mathrm{RW}} \\ \eta_{\mathrm{LW}} \end{bmatrix} \tag{66}$$

The matrices $\mathbf{B_{A1}}$ and $\mathbf{B_{A2}}$ are explicitly expressed as

$$\mathbf{B_{A1}} = \begin{bmatrix} 0 & 0 & \left.\frac{\partial \bar{F}^B_{x\mathrm{RW}}}{\partial \omega_{\mathrm{RW}}}\right|_{\mathrm{hover}} & \left.\frac{\partial \bar{F}^B_{x\mathrm{LW}}}{\partial \omega_{\mathrm{LW}}}\right|_{\mathrm{hover}} & \left.\frac{\partial \bar{F}^B_{x\mathrm{RW}}}{\partial \eta_{\mathrm{RW}}}\right|_{\mathrm{hover}} & \left.\frac{\partial \bar{F}^B_{x\mathrm{LW}}}{\partial \eta_{\mathrm{LW}}}\right|_{\mathrm{hover}} \\ 0 & 0 & 0 & 0 & \left.\frac{\partial \bar{F}^B_{y\mathrm{RW}}}{\partial \eta_{\mathrm{RW}}}\right|_{\mathrm{hover}} & \left.\frac{\partial \bar{F}^B_{y\mathrm{LW}}}{\partial \eta_{\mathrm{LW}}}\right|_{\mathrm{hover}} \\ \left.\frac{\partial \bar{F}^B_{z\mathrm{RW}}}{\partial \delta_{\mathrm{RW}}}\right|_{\mathrm{hover}} & \left.\frac{\partial \bar{F}^B_{z\mathrm{LW}}}{\partial \delta_{\mathrm{LW}}}\right|_{\mathrm{hover}} & 0 & 0 & \left.\frac{\partial \bar{F}^B_{z\mathrm{RW}}}{\partial \eta_{\mathrm{RW}}}\right|_{\mathrm{hover}} & \left.\frac{\partial \bar{F}^B_{z\mathrm{LW}}}{\partial \eta_{\mathrm{LW}}}\right|_{\mathrm{hover}} \\ \left.\frac{\partial \bar{M}^B_{x\mathrm{RW}}}{\partial \delta_{\mathrm{RW}}}\right|_{\mathrm{hover}} & \left.\frac{\partial \bar{M}^B_{x\mathrm{LW}}}{\partial \delta_{\mathrm{LW}}}\right|_{\mathrm{hover}} & 0 & 0 & \left.\frac{\partial \bar{M}^B_{x\mathrm{RW}}}{\partial \eta_{\mathrm{RW}}}\right|_{\mathrm{hover}} & \left.\frac{\partial \bar{M}^B_{x\mathrm{LW}}}{\partial \eta_{\mathrm{LW}}}\right|_{\mathrm{hover}} \\ \left.\frac{\partial \bar{M}^B_{y\mathrm{RW}}}{\partial \delta_{\mathrm{RW}}}\right|_{\mathrm{hover}} & \left.\frac{\partial \bar{M}^B_{y\mathrm{LW}}}{\partial \delta_{\mathrm{LW}}}\right|_{\mathrm{hover}} & 0 & 0 & \left.\frac{\partial \bar{M}^B_{y\mathrm{RW}}}{\partial \eta_{\mathrm{RW}}}\right|_{\mathrm{hover}} & \left.\frac{\partial \bar{M}^B_{y\mathrm{LW}}}{\partial \eta_{\mathrm{LW}}}\right|_{\mathrm{hover}} \\ 0 & 0 & \left.\frac{\partial \bar{M}^B_{z\mathrm{RW}}}{\partial \omega_{\mathrm{RW}}}\right|_{\mathrm{hover}} & \left.\frac{\partial \bar{M}^B_{z\mathrm{LW}}}{\partial \omega_{\mathrm{LW}}}\right|_{\mathrm{hover}} & \left.\frac{\partial \bar{M}^B_{z\mathrm{RW}}}{\partial \eta_{\mathrm{RW}}}\right|_{\mathrm{hover}} & \left.\frac{\partial \bar{M}^B_{z\mathrm{LW}}}{\partial \eta_{\mathrm{LW}}}\right|_{\mathrm{hover}} \end{bmatrix} \tag{67}$$

and

$$\mathbf{B_{A2}} = -\begin{bmatrix} \left.\frac{\partial \bar{F}^B_{x\mathrm{RW}}}{\partial \eta_{\mathrm{RW}-1}}\right|_{\mathrm{hover}} & \left.\frac{\partial \bar{F}^B_{x\mathrm{LW}}}{\partial \eta_{\mathrm{LW}-1}}\right|_{\mathrm{hover}} \\ \left.\frac{\partial \bar{F}^B_{y\mathrm{RW}}}{\partial \eta_{\mathrm{RW}-1}}\right|_{\mathrm{hover}} & \left.\frac{\partial \bar{F}^B_{y\mathrm{LW}}}{\partial \eta_{\mathrm{LW}-1}}\right|_{\mathrm{hover}} \\ \left.\frac{\partial \bar{F}^B_{z\mathrm{RW}}}{\partial \eta_{\mathrm{RW}-1}}\right|_{\mathrm{hover}} & \left.\frac{\partial \bar{F}^B_{z\mathrm{LW}}}{\partial \eta_{\mathrm{LW}-1}}\right|_{\mathrm{hover}} \\ \left.\frac{\partial \bar{M}^B_{x\mathrm{RW}}}{\partial \eta_{\mathrm{RW}-1}}\right|_{\mathrm{hover}} & \left.\frac{\partial \bar{M}^B_{x\mathrm{LW}}}{\partial \eta_{\mathrm{LW}-1}}\right|_{\mathrm{hover}} \\ \left.\frac{\partial \bar{M}^B_{y\mathrm{RW}}}{\partial \eta_{\mathrm{RW}-1}}\right|_{\mathrm{hover}} & \left.\frac{\partial \bar{M}^B_{y\mathrm{LW}}}{\partial \eta_{\mathrm{LW}-1}}\right|_{\mathrm{hover}} \\ \left.\frac{\partial \bar{M}^B_{z\mathrm{RW}}}{\partial \eta_{\mathrm{RW}-1}}\right|_{\mathrm{hover}} & \left.\frac{\partial \bar{M}^B_{z\mathrm{LW}}}{\partial \eta_{\mathrm{LW}-1}}\right|_{\mathrm{hover}} \end{bmatrix} \tag{68}$$

From the structure of $\mathbf{B_{A1}}$ and the expressions for its elements found in Eqs. (36–62), it is found that this matrix has a rank of six. Hence, SCCPFM with wing bias has provided a technique to control 6 DOFs with only two physical actuators. Fundamental frequency (ω_{RW} and ω_{LW}) can be used to control the x-body axis force and yawing moment. Likewise, the split-cycle parameters ($\delta_{\mathrm{RW}}, \delta_{\mathrm{LW}}$) can be used to control rolling moment and either z-body axis force or pitching moment. The primary function of the wing bias parameters is to replace the bobweight [12] as a pitching-moment control parameter. Additionally, the wing bias allows the ability to generate side forces. The control allocation objective is to find the control vector,

$$[\,\delta_{\mathrm{RW}} \quad \delta_{\mathrm{LW}} \quad \Delta\omega_{\mathrm{RW}} \quad \Delta\omega_{\mathrm{LW}} \quad \eta_{\mathrm{RW}} \quad \eta_{\mathrm{LW}}\,]^T$$

such that Eq. (66) is satisfied. The desired forces and moments in Eq. (66) are generated by a feedback structure designed to track a desired trajectory. The control allocation scheme is a pseudoinverse, and the control vector is computed as

$$\mathbf{B_{A1}}^{+}\left\{\begin{bmatrix}\Delta\bar{F}^B_{x\mathrm{des}}\\ \Delta\bar{F}^B_{y\mathrm{des}}\\ \Delta\bar{F}^B_{z\mathrm{des}}\\ \Delta\bar{M}^B_{x\mathrm{des}}\\ \Delta\bar{M}^B_{y\mathrm{des}}\\ \Delta\bar{M}^B_{z\mathrm{des}}\end{bmatrix} - \mathbf{B_{A2}}\begin{bmatrix}-\eta_{\mathrm{RW}-1}\\ -\eta_{\mathrm{LW}-1}\end{bmatrix}\right\} = \begin{bmatrix}\delta_{\mathrm{RW}}\\ \delta_{\mathrm{LW}}\\ \Delta\omega_{\mathrm{RW}}\\ \Delta\omega_{\mathrm{LW}}\\ \eta_{\mathrm{RW}}\\ \eta_{\mathrm{LW}}\end{bmatrix} \tag{69}$$

where $\mathbf{B_{A1}}^{+}$ is the pseudoinverse of $\mathbf{B_{A1}}$. The control values, in Eq. (69), are held constant over a wingbeat cycle and are applied to oscillators that generate the wingbeat forcing functions.

VII. Results

The modeling and control analysis is now used in a 6-DOF model of the flapping-wing MAV. The control design approach is the same as that used by Doman et al. [12] with the bobweight pitch loop replaced by wing bias loops. This controller is chosen to facilitate a direct comparison between the results in this work and those presented by Doman et al. [12]. The controller actively controls only 5 DOFs because the bobweight vehicle configuration only provided up to 5-DOF control. Specifically, the controller does not generate a desired side translational force. Therefore, this controller only makes use of five of the possible 6-DOF controls provided by the wing bias configuration.

Figure 5 shows the structure of the controller. In Fig. 5, the blocks labeled MUX are multiplexers, EOM denotes equations of motion, and ZOH denotes zero-order hold. Position and attitude errors generate all desired accelerations (or forces and moments). The control allocation problem in Eq. (69) is then solved to provide the control vector. Recall that the output of the control allocation is actually an increment to right and left fundamental frequency. Hence, implicit in Fig. 5 is the addition of the trim frequency to the control allocation output to obtain ω_{RW} and ω_{LW}. After being held constant for each complete wingbeat cycle, the control variables are inputs to oscillators that provide the wingbeat forcing functions. The forcing functions are inputs to an aerodynamic model of the vehicle, and 6-DOF equations of motion are integrated to obtain the state of the vehicle. A simulation was performed with the 6-DOF model driven by the instantaneous forces and moments from the model that includes wing flapping, rigid-body translation and rotation, and the experimentally derived lift and drag coefficients from Sane and Dickinson [5]. The simulation results show the commanded time history and the actual response. The instantaneous aerodynamic model that includes the effects of wing flapping, rigid-body translation and rotation, and the experimental lift and drag coefficients, was not used in the controller design and is only used as the truth model. Thus, there is an inherent modeling error between the simulation model and the model used to design the control law, and the controller must be robust enough to tolerate this error.

Table 2 Vehicle parameters used in simulation

Variable	Value
Mass, mg	90
Height, width, depth, mm	14, 8, 3
Center of gravity location, mm	[7 0 0]
c, b, and R, mm	4, 3, 15
$\Delta\mathbf{r}^B_{\mathrm{RW}}$, mm	[2 4 0]
$\Delta\mathbf{r}^B_{\mathrm{LW}}$, mm	[2 −4 0]
Angle between stoke plane and wing chord (α), deg	45
Hover frequency $= \omega_o = \sqrt{\mathrm{weight}/0.5\rho C_L(\alpha) I_A}$, rad/s	754

Table 2 displays the vehicle parameters that were used during the simulation. The center-of-gravity location is taken to be the geometric center of the vehicle, and all variables are defined by Doman et al. [12].

The commanded trajectory for the presented simulation run is shown in Fig. 6. The vehicle starts by executing a roll to align its heading with waypoint 1 as it performs a translation in the direction of the y axis of the inertial frame toward waypoint 1. After arriving at waypoint 1, the vehicle aligns its heading with waypoint 2 as it translates in both the x-axis and z-axis directions of the inertial frame on its way to waypoint 2. Two constant altitude maneuvers are made in moving to waypoints 3 and 4, followed by a change in altitude to get to waypoint 5, the final waypoint.

Figure 7 shows the commanded and actual roll, pitch, and yaw angles of the MAV during the flight, while Fig. 8 shows the commanded and actual positions of the vehicle. The large roll angles are used to align the heading of the vehicle with the next waypoint, while for forward translation, a nonzero pitch attitude angle is used. The position errors are small, and the vehicle is capable of tracking the commanded trajectory.

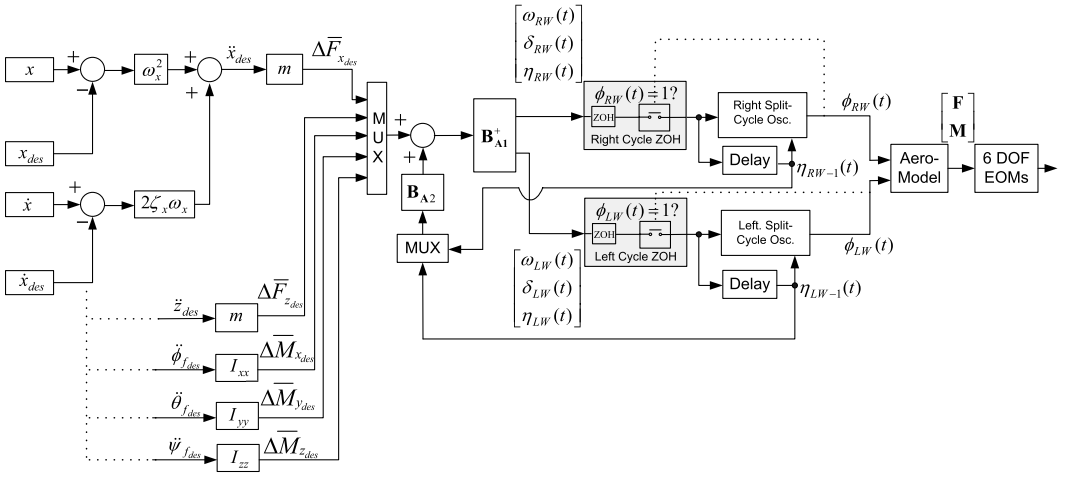

Fig. 5 Five-DOF split-cycle controller with wing bias.

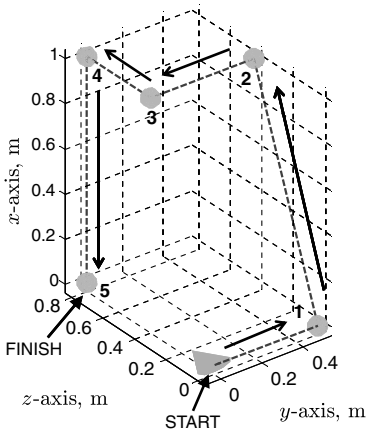

Fig. 6 Commanded MAV trajectory.

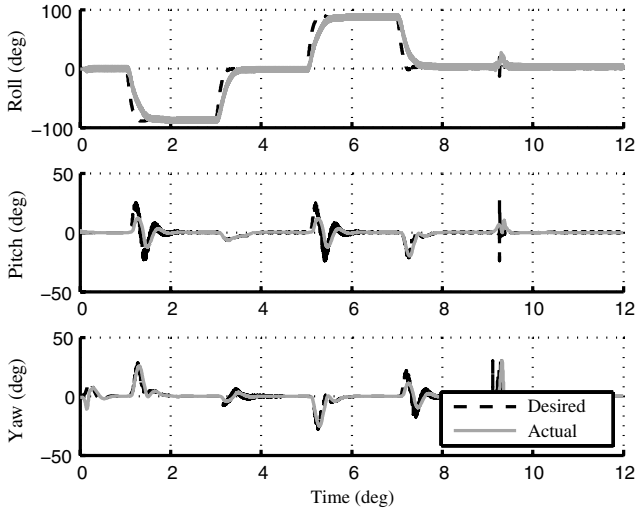

Fig. 7 Vehicle attitude.

Figures 9–11 show the values of the control variables required to produce this maneuver. The trim wingbeat frequency is about 120 Hz, with large excursions during the portions of the flight where altitude changes are made. Recall that fundamental frequency has a large effect on vertical force so, as expected, large variations in ω occur during the flight from waypoints 1 to 2 and from waypoints 4 to 5. The split-cycle parameter is used to produce roll and force in the

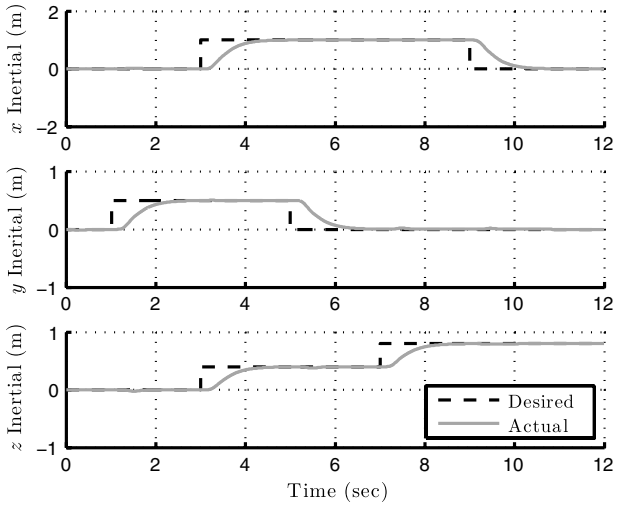

Fig. 8 Vehicle position.

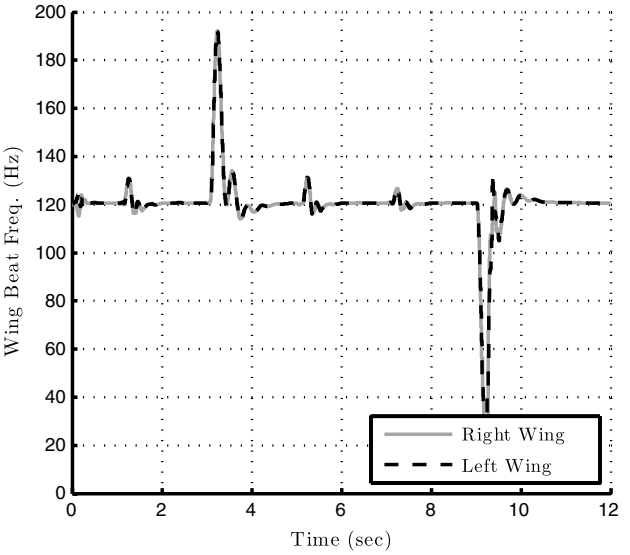

Fig. 9 Fundamental wingbeat frequency ω.

z-body axis direction and is therefore active during all portions of this flight. Notice that in moving from waypoints 4 to 5 (just past 9 s), the split-cycle parameter is active, even though no fore/aft translation or heading correction is required. Additionally, the split-cycle parameter displays high-frequency oscillatory behavior, which would not be present if the simplified blade-element aerodynamic model were used as the truth model. This is due to the modeling error introduced by using a simplified aerodynamic model to develop the controller. The bias is used to regulate the pitch of the vehicle and is active during all portions of the flight. One interesting point is that a bias value of about 3 deg is sufficient to regulate the attitude. The high-frequency wing bias at about 9 s is due to the pitching moment being coupled between the split-cycle parameter and wing bias, unmodeled dynamics, and the fact that the control effectiveness parameters are evaluated at hover. Referring to Fig. 9, it is evident that during this maneuver (from waypoints 4 to 5) the fundamental frequency is far from the hover value of 120 Hz. Equations (53) and (55) show that the cycle-averaged pitching moment due to wing bias is a function of the square of the fundamental frequency. Hence, when the fundamental frequency experiences a large change from the hover frequency, the control effectiveness parameters are incorrect and introduce modeling errors. Fortunately, the controller is robust to this error.

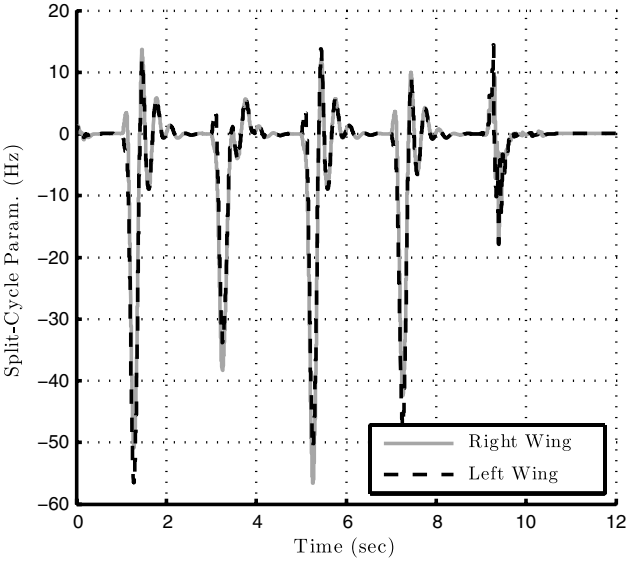

Fig. 10 Split-cycle parameter δ.

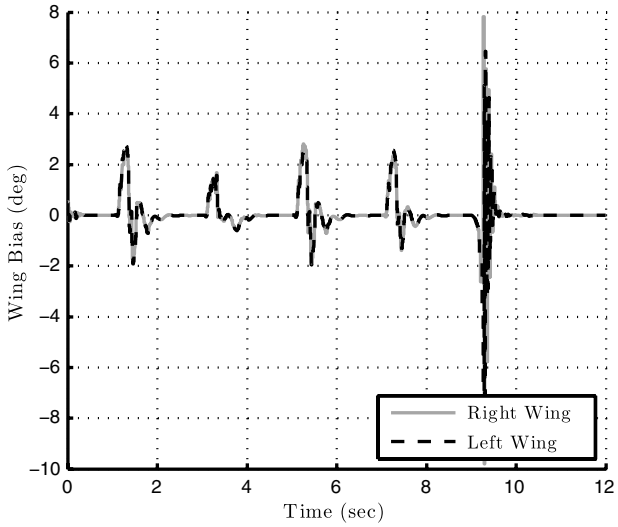

Fig. 11 Wing bias η.

VIII. Conclusions

The analysis shows that the use of SCCPFM with wing bias and independently actuated wings allows manipulation of the x-, y-, and z-body axes forces as well as the rolling, pitching, and yawing moments. Cycle-averaged forces, rolling moment, and yawing moment are only produced by the wing bias when there is a difference between the wing bias on successive wingbeat cycles. In terms of the pitching moment, any nonzero wing bias will produce a persistent moment about the y-body axis. Thus, the primary effect of wing bias is in the production of pitching moment, and a bobweight is not needed. The addition of a wing bias to the SCCPFM technique yields 6-DOF control using only two physical actuators. Given the ability to manipulate the cycle-averaged body axes forces and moments, untethered controlled flight with insectlike maneuverability appears to be feasible with only two physical actuators. Furthermore, the results indicate that controllers based on cycle-averaged blade-element aerodynamic models, for this class of vehicle, are robust to modeling errors caused by the presence of rigid-body translation and rotation.

Acknowledgment

This research was performed while David O. Sigthorsson held a National Research Council Research Associateship Award at the Air Force Research Laboratory.

References

[1] Osborne, M. F. M., "Aerodynamics of Flapping Flight with Application to Insects," *Journal of Experimental Biology*, Vol. 28, No. 2, 1951, pp. 221–245.

[2] Jensen, M., "Biology and Physics of Locust Flight III: The Aerodynamics of Locust Flight," *Philosophical Transactions of the Royal Society of London Series B, Biological Series*, Vol. 239, No. 667, 1956, pp. 511–552. doi:10.1098/rstb.1956.0009.

[3] Vogel, S., "Flight in Drosophila II: Variations in Stroke Parameters and Wing Contour," *Journal of Experimental Biology*, Vol. 46, No. 2, 1967, pp. 383–392.

[4] Vogel, S., "Flight in Drosophila III: Aerodynamic Characteristics of Fly Wings and Wing Models," *Journal of Experimental Biology*, Vol. 46, No. 3, 1967, pp. 431–443.

[5] Sane, S. P., and Dickinson, M. H., "The Control of Flight Force by a Flapping Wing: Lift and Drag Production," *Journal of Experimental Biology*, Vol. 204, No. 15, 2001, pp. 2607–2626.

[6] Sane, S. P., and Dickinson, M. H., "The Aerodynamic Effects of Wing Rotation and a Revised Quasi-Steady Model of Flapping Flight," *Journal of Experimental Biology*, Vol. 205, 2002, pp. 1087–1096.

[7] Wood, R. J., "The First Takeoff of a Biologically Inspired At-Scale Robotic Insect," *IEEE Transactions on Robotics*, Vol. 24, No. 2, 2008, pp. 341–347. doi:10.1109/TRO.2008.916997

[8] Wood, R. J., "Design, Fabrication, and Analysis of a 3DOF, 3 cm Flapping-Wing MAV," *Proceedings of the 2007 IEEE/RSJ International Conference on Intelligent Robots and Systems*, IEEE Publ., Piscataway, NJ, Oct. 2007, pp. 1576–1581. doi:10.1109/IROS.2007.4399495

[9] Ellington, C. P., "The Aerodynamics of Hovering Insect Flight. I: The Quasi-Steady Analysis," *Philosophical Transactions of the Royal Society of London Series B, Biological Series*, Vol. 305, No. 1122, 1984, pp. 1–15. doi:10.1098/rstb.1984.0049

[10] Dudley, R., and Ellington, C. P., "Mechanics of Forward Flight in Bumblebees I: Kinematics and Morphology," *Journal of Experimental Biology*, Vol. 148, No. 1, 1990, pp. 19–52.

[11] Dudley, R., and Ellington, C. P., "Mechanics of Forward Flight in Bumblebees II: Quasi-Steady Lift and Power Requirements," *Journal of Experimental Biology*, Vol. 148, No. 1, 1990, pp. 53–88.

[12] Doman, D. B., Oppenheimer, M. W., and Sigthorsson, D. O., "Wingbeat Shape Modulation for Flapping-Wing Micro-Air-Vehicle Control During Hover," *Journal of Guidance, Control, and Dynamics*, Vol. 33, No. 3, 2010, pp. 724–739. doi:10.2514/1.47146

[13] Deng, X., Schenato, L., and Sastry, S. S., "Flapping Flight for Biomimetic Robotic Insects: Part II, Flight Control Design," *IEEE Transactions on Robotics*, Vol. 22, No. 4, 2006, pp. 789–803. doi:10.1109/TRO.2006.875483

[14] Ellington, C. P., "The Aerodynamics of Hovering Insect Flight. II. Morphological Parameters," *Philosophical Transactions of the Royal Society of London Series B, Biological Series*, Vol. 305, No. 1122, 1984, pp. 17–40. doi:10.1098/rstb.1984.0050

[15] Ellington, C. P., "The Aerodynamics of Hovering Insect Flight. III. Kinematics," *Philosophical Transactions of the Royal Society of London Series B, Biological Series*, Vol. 305, No. 1122, 1984, pp. 41–78. doi:10.1098/rstb.1984.0051

[16] Ellington, C. P., "The Aerodynamics of Hovering Insect Flight. IV. Aerodynamic Mechanisms," *Philosophical Transactions of the Royal Society of London Series B, Biological Series*, Vol. 305, No. 1122, 1984, pp. 79–113. doi:10.1098/rstb.1984.0052

[17] Ellington, C. P., "The Aerodynamics of Hovering Insect Flight. V. A Vortex Theory," *Philosophical Transactions of the Royal Society of London Series B, Biological Series*, Vol. 305, No. 1122, 1984, pp. 115–144. doi:10.1098/rstb.1984.0053

[18] Ellington, C. P., "The Aerodynamics of Hovering Insect Flight. VI. Lift and Power Requirements," *Philosophical Transactions of the Royal Society of London Series B, Biological Series*, Vol. 305, No. 1122, 1984, pp. 145–181. doi:10.1098/rstb.1984.0054

[19] Dudley, R., "Biomechanics of Flight in Neotropical Butterflies: Aerodynamics and Mechanical Power Requirements," *Journal of Experimental Biology*, Vol. 159, No. 1, 1991, pp. 335–357.

[20] Ennos, A. R., "The Kinematics and Aerodynamics of the Free Flight of Some Diptera," *Journal of Experimental Biology*, Vol. 142, No. 1, 1989, pp. 49–85.

[21] Willmott, A. P., and Ellington, C. P., "The Mechanics of Flight in the Hawkmoth *Manduca Sexta* I. Kinematics of Hovering and Forward Flight," *Journal of Experimental Biology*, Vol. 200, No. 21, 1997, pp. 2705–2722.

[22] Willmott, A. P., and Ellington, C. P., "The Mechanisms of Flight in the Hawkmoth *Manduca Sexta* II. Aerodynamic Consequences of Kinematic and Morphological Variation," *Journal of Experimental Biology*, Vol. 200, No. 21, 1997, pp. 2723–2745.

[23] Willmott, A. P., Ellington, C. P., and Thomas, A. L. R., "Flow Visualization and Unsteady Aerodynamics in the Flight of the Hawkmoth *Manduca Sexta*," *Philosophical Transactions of the Royal Society of London Series B, Biological Series*, Vol. 352, No. 1351, 1997, pp. 303–316. doi:10.1098/rstb.1997.0022

[24] Shyy, W., Lain, Y., Tang, J., Viieru, D., and Lui, H., *Aerodynamics of Low Reynolds Number Flyers*, Cambridge Univ. Press, New York, NY, 2008, p. 6.

[25] Deng, X., Schenato, L., Wu, W. C., and Sastry, S. S., "Flapping Flight for Biomimetic Robotic Insects: Part I: System Modeling," *IEEE Transactions on Robotics*, Vol. 22, No. 4, 2006, pp. 776–788. doi:10.1109/TRO.2006.875480

[26] Żbikowski, R., "On Aerodynamic Modelling of an Insect-Like Flapping Wing in Hover for Micro Air Vehicles," *Philosophical Transactions of the Royal Society of London: Series A*, Vol. 360, No. 1791, 2002, pp. 273–290. doi:10.1098/rsta.2001.0930

[27] Sane, S. P., "The Aerodynamics of Insect Flight," *Journal of Experimental Biology*, Vol. 206, No. 23, 2003, pp. 4191–4208. doi:10.1242/jeb.00663

[28] Dickinson, M. H., and Götz, K. G., "Unsteady Aerodynamic Performance of Model Wings at Low Reynolds Numbers," *Journal of Experimental Biology*, Vol. 174, No. 1, 1993, pp. 45–64.

[29] Sitaraman, J., Roget, B., Harmon, R., Graurer, J., Conroy, J., Hubbard, J., and Humbert, S., "A Computational Study of Flexible Wing Ornithopter Flight," AIAA Paper 2008-6397, Aug. 2008.

[30] Deng, X., Schenato, L., and Sastry, S. S., "Hovering Flight Control of a Micromechanical Flying Insect," *IEEE Conference on Decision and Control*, Vol. 1, IEEE Publ., Piscataway, NJ, Dec. 2001, pp. 235–240. doi:10.1109/.2001.980104

[31] Doman, D. B., Oppenheimer, M. W., and Bolender, M. A., "Altitude Control of a Single Degree of Freedom Flapping Wing Micro Air Vehicle," AIAA Paper 2009-6159, Aug. 2009.

[32] Wood, R. J., Steltz, E., and Fearing, R. S., "Optimal Energy Density Piezoelectric Bending Actuators," *Sensors and Actuators. A, Physical*, Vol. 119, No. 2, 2005, pp. 476–488. doi:10.1016/j.sna.2004.10.024

[33] Hedrick, T. L., Cheng, B., and Deng, X., "Wingbeat Time and the Scaling of Passive Rotational Damping in Flapping Flight," *Science*, Vol. 324, No. 5924, 2009, pp. 252–255. doi:10.1126/science.1168431

[34] Faruque, I., and Humbert, J. S., "Dipterian Insect Flight Dynamics. Part 1 Longitudinal Motion About Hover," *Journal of Theoretical Biology*, Vol. 264, No. 2, 2010, pp. 538–552. doi:10.1016/j.jtbi.2010.02.018

[35] Gradshteyn, I. S., and Ryzhik, I. M., *Table of Integrals*, Series and Products, 6th ed., Academic Press, New York, 2000, pp. 414–415, 932.

[36] Oppenheimer, M. W., Doman, D. B., and Sigthorsson, D. O., "Dynamics and Control of a Biomimetic Vehicle Using Biased Wingbeat Forcing Functions: Part I: Aerodynamic Model," AIAA Paper 2010-1023, Jan. 2010.

[37] Doman, D. B., Oppenheimer, M. W., and Sigthorsson, D. O., "Dynamics and Control of a Biomimetic Vehicle Using Biased Wingbeat Forcing Functions: Part II: Controller," AIAA Paper 2010-1024, Jan. 2010.